

Affordance-Graphed Task Worlds: Self-Evolving Task Generation for Scalable Embodied Learning

Xiang Liu ^{*} Sen Cui ^{*†} Guocai Yao Zhong Cao Jingheng Ma Min Zhang Changshui Zhang [†]

Abstract

Training robotic policies directly in the real world is expensive and unscalable. Although generative simulation enables large-scale data synthesis, current approaches often fail to generate logically coherent long-horizon tasks and struggle with dynamic physical uncertainties due to open-loop execution. To address these challenges, we propose Affordance-Graphed Task Worlds (AGT-World), a unified framework that autonomously constructs interactive simulated environments and corresponding robot task policies based on real-world observations. Unlike methods relying on random proposals or static replication, AGT-World formalizes the task space as a structured graph, enabling the precise, hierarchical decomposition of complex goals into theoretically grounded atomic primitives. Furthermore, we introduce a Self-Evolution mechanism with hybrid feedback to autonomously refine policies, combining Vision-Language Model reasoning and geometric verification. Extensive experiments demonstrate that our method significantly outperforms in success rates and generalization, achieving a self-improving cycle of proposal, execution, and correction for scalable robot learning. ¹

1. Introduction

Training general-purpose robotic policies directly in the real world remains expensive, unsafe, and difficult to scale. Consequently, leveraging large-scale synthetic data within simulation has emerged as a promising alternative to overcome the scarcity of real-world demonstrations.

Recent advances in world models and video generation have significantly improved visual fidelity. However, they

are typically trained without explicit physical supervision, often producing physically inconsistent outcomes such as floating objects or interpenetration. This limits their direct applicability to robotics, where physical plausibility is paramount (Li et al., 2025b; Meng et al., 2024; Kang et al., 2024). To ensure physical feasibility, the embodied AI community relies on physics simulators that provide precise collision handling and interaction feedback. Existing approaches often trade off between diversity and realism: random placement lacks logical layout, while digital twin reconstruction is prohibitively expensive. We adopt a balanced approach, reconstructing interactive environments that preserve the semantic and functional layout of real-world observations using matched assets (Dai et al., 2024).

Even within these valid interactive scenes, automating task planning and execution remains fraught with challenges. Previous works often rely on hard-coded heuristics or “black-box” reinforcement learning (RL) exploration, which frequently suffer from sparse rewards and low success rates (Wang et al., 2024). The challenge is particularly acute in long-horizon tasks, because open-loop execution pipelines of previous work fail to adapt to dynamic uncertainties. A minor error in the early stages can accumulate, leading to total failure, as illustrated in Figure 1.

To address these limitations, we propose Affordance-Graphed Task Worlds (AGT-World), a unified framework that autonomously constructs interactive environments and generates physically feasible, semantically consistent long-horizon tasks. Our approach is based on the framework (Dai et al., 2024) to reconstruct simulation scenes from single RGB images, preserving semantic affordances and object states. We model the task space as a structured graph, enabling precise decomposition of complex goals into atomic primitives. Crucially, we introduce a closed-loop self-evolution mechanism to refine policies. We summarize our key contributions as follows:

- **Bridging the Semantic-Physical Gap:** We reconstruct diverse simulated scenes that preserve both geometric layouts and semantic affordances of real-world scenes, bridging the gap between visual perception and physical simulation assets, ensuring that generated data is not just visually diverse but functionally actionable.

^{*}Equal contribution. Correspondence to: Sen Cui <cuis@mail.tsinghua.edu.cn>, Changshui Zhang <zcs@mail.tsinghua.edu.cn>.

[†]Our project page at: <https://agt-world.github.io/>

¹Our project page at: <https://agt-world.github.io/>

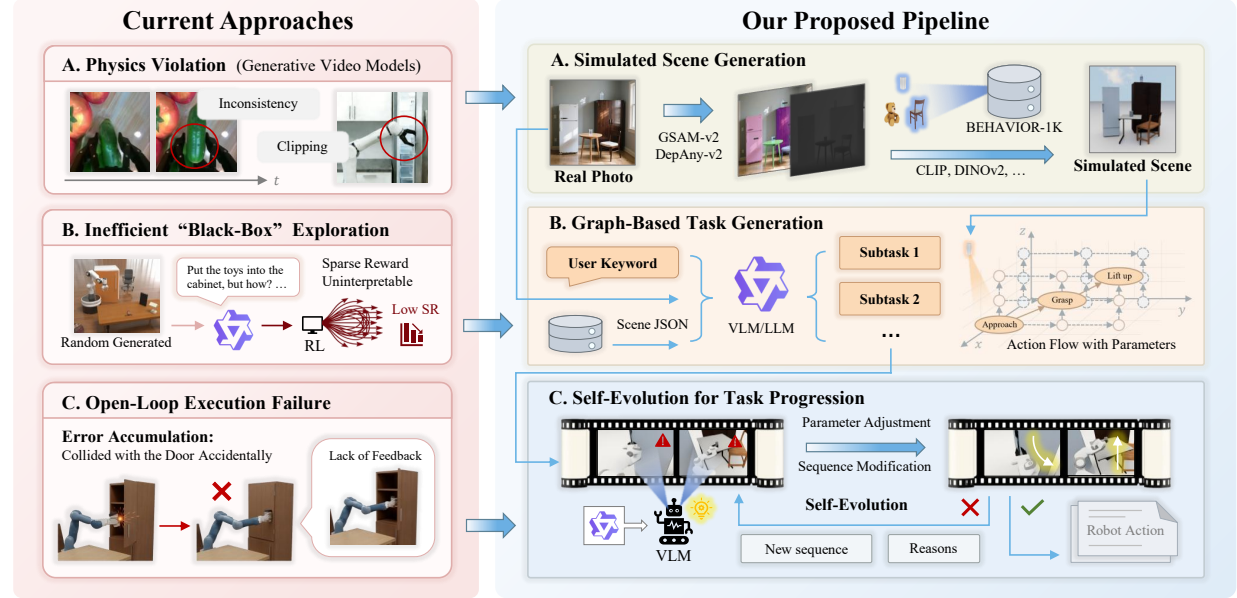


Figure 1. An introduction of our method. **A.** Video generation models often produce physically implausible behaviors. We instead employ a **physics simulation engine** to reconstruct semantic and global-state preserving simulated scenes from real-world images at low cost. **B.** Randomly generated scenes are far from realism, and RL suffers from sparse rewards. We adopt **affordance-graphed task generation**, which enables planning and execution of action sequences in arbitrary scenes. **C.** In long-horizon tasks, policies typically lack execution feedback leading to error accumulation. We introduce **VLM-supervised self-evolution** to iteratively correct task actions during execution.

- **Unified Generation and Self-Evolving Framework:**

We formalize the task generation process as a path-planning problem within a structured AGT-World. By integrating scene reconstruction with this graph-theoretic modeling, we introduce a closed-loop Self-Evolution mechanism. This mechanism utilizes VLM-guided hybrid feedback to autonomously diagnose execution failures and refine parameters.

- **Scalable Generation and Superior Performance:**

Extensive experiments in 102 autonomously generated scene-task pairs demonstrate that our method achieves a high overall success rate of **71.6%**. We also demonstrate the effectiveness of our self-evolving mechanism in 4 complex long-horizon tasks involving multiple primary tasks categories.

2. Related Works

In this section, we will review various approaches that aim to scaling up embodied data generation and policy learning.

Generative Video Models and Simulators. Early works like VideoGPT (Yan et al., 2021) laid the foundation for latent video synthesis. More recently, foundation models such as Genie (Bruce et al., 2024; Liao et al., 2025) and Sora (Liu et al., 2024) have achieved unprecedented fidelity in video prediction and interactive scene modeling. However, as noted in recent benchmarks (Li et al., 2025b), they operate without an underlying physics engine.

To provide physically grounded training data, high-fidelity simulators such as OmniGibson (Li et al., 2023), Genesis (Zhou et al., 2024), iGibson (Li et al., 2022), ManiSkill (Tao et al., 2025), and ThreeDWorld (Gan et al., 2020) have been developed. We utilize OmniGibson in our framework due to its rich interaction capabilities and support for realistic object states, which is powered by Isaac Sim (Makoviychuk et al., 2021).

Scene Reconstruction and Task Generation. Some previous works use procedural generation or text-to-scene methods like Holodeck (Yang et al., 2024b) and RoboGen (Wang et al., 2024), they generate layouts from LLMs, but often lack visual fidelity to specific real-world references. While GRS (Zook et al., 2025) and EmbodiedGen (Wang et al., 2025) can construct a digital twin simulation from a single RGB-D observation, but they incurs a high cost. Conversely, reconstruction techniques using NeRFs or 3D Gaussian Splatting offer photorealism but result in static non-interactive scenes (Kerbl et al., 2023; Kerr et al., 2023).

Scaling robotic learning requires not just scenes, but valid tasks. While digital cousins policy (Dai et al., 2024) reduces the cost of digital twin creation but restricts itself to predefined tasks. Recent automated works like RoboGen (Wang et al., 2024), GenSim2 (Hua et al., 2024) and ReGen (Nguyen et al., 2025) leverage Multi-modal LLMs to propose tasks and generate corresponding training code. In addition, some work like GRS (Zook et al., 2025) leverages a VLM for task generation.

Policy Learning and VLA Models. Recent works like RoboGen (Wang et al., 2024), Eureka (Ma et al., 2024b) and DrEureka (Ma et al., 2024a) leverage LLMs to automate reward design for RL, they often remain sensitive to exploration efficiency in sparse-reward settings. Conversely, approaches like MimicGen (Garrett et al., 2024) and Scaling Robot Learning (Yu et al., 2023) focus on scaling imitation learning via synthesized demonstrations. Similarly, MomaGen (Li et al., 2025a) attempts to generate demonstrations under soft and hard constraints to train policies.

Currently, end-to-end Vision-Language-Action (VLA) models such as RT-2 (Zitkovich et al., 2023), OpenVLA (Kim et al., 2024), and Octo (Mees et al., 2024) have shown great promise. These models excel at fine-grained articulated manipulation and handling complex spatial relationships. In addition, recent work has demonstrated the efficacy of VLAs in specific contexts (Tao et al., 2025; Yang et al., 2025; Zhen et al., 2024; O’Neill et al., 2024). However, these VLA models typically function as open-loop executors and struggle with long-horizon reasoning.

Our framework providing a high-level, graph-based planning structure with self-evolution verification, where closed-loop policies are inspired by recent iterative improvement strategies (Tian et al., 2025; Garrett et al., 2024). In the future, we can also effectively complement VLAs by utilizing AGT-World as global policy executors for manipulation, analogous to hierarchical architectures in AutoRT (Ahn et al., 2024) and CoPa (Huang et al., 2024).

3. Preliminary

Before demonstrating our task world modeling and algorithm implementation, we need to first introduce some basic concepts. In this section, we present methods for generating simulated scenes and tasks definition.

3.1. Simulated Scene Generation

The generation of the simulation environment reconstructs an interactive scene from a single real-world RGB observation. Specifically, let \mathcal{S} denote the universal physical state space of the environment, where each element $s_\tau \in \mathcal{S}$ represents a possible relationship between any two objects at time τ , and $X_0 \in \mathbb{R}^{H \times W \times 3}$ denote the real-world input image. The process outputs a simulated initial state $S_0 \subset \mathcal{S}$, which is modeled as a sample from a posterior distribution conditioned on the visual input:

$$S_0 \sim p(S \mid X_0; \epsilon_0), \quad (1)$$

where ϵ_0 encapsulates the reconstruction error inherited within the reconstruction pipeline. For the complete simulated scene generation process and some examples of state definition, refer to Appendix A.1, A.2.3.

3.2. Simple Task Definitions

To rigorously define the boundaries of decomposition, we categorize tasks into *Simple Tasks* and *Complex Long-Horizon Tasks*.

Object Roles and Simple Task Tuple. First, we define the core elements of any simple manipulation task unit. We denote o_t as the target object, and o_{s_1}, o_{s_2} as the initial and goal support objects, respectively. The states of initialization and termination are defined as functions of these objects:

$$s_{\text{init}} = s_{\text{init}}(o_t, o_{s_1}), s_{\text{goal}} = s_{\text{goal}}(o_t, o_{s_2}) \in \mathcal{S}. \quad (2)$$

Here, o_t is the direct object of the robot’s action sequence and must exist. If o_t is a fixed object, its attributes usually represent specific parts, such as a handle; otherwise, it typically represents the object itself. o_{s_1} defines the precondition constraints of o_t , and o_{s_2} defines the success criteria of o_t . For tasks involving only state changes of o_t itself, the support o_{s_1} and o_{s_2} may all be null.

Then we can give the definition of the *Simple Task*:

Definition 3.1 (Simple Task). A task T is defined as simple task and we denote as

$$T = \langle o_t, o_{s_1}, o_{s_2}, s_{\text{init}}, s_{\text{goal}} \rangle. \quad (3)$$

Action Flow and Generative Uncertainty. A simple task T is executed via an *Action Flow*, denoted as

$$\pi(T) = \{a_1(o_t), a_2(o_t), \dots, a_n(o_t)\}, \quad (4)$$

representing a sequence of n atomic primitives $\{a_i\}_{i=1}^n$ acting upon the target object o_t . In our generative framework, the optimal action flow is not deterministic but is modeled as a sample from a posterior distribution conditioned on the task definition, governed by a LLM:

$$\pi \sim p_F(\pi \mid T; \epsilon_1), \quad (5)$$

where ϵ_1 represents the aleatoric uncertainty and generative error inherent in the LLM’s reasoning process. A task T is valid if there exists at least an action flow π_n satisfies (5), which ensures the transition from s_{init} to s_{goal} while maintaining invariance in the unmodelled subspace of \mathcal{S} , that is, $\mathbb{P}(s_{\text{goal}} \mid s_{\text{init}}, \pi) > 0$.

3.3. Complex Long-Horizon Tasks and Decomposition

Definition 3.2 (Complex Long-Horizon Task). A complex long-horizon task \mathcal{T} is defined as an ordered sequence of simple tasks:

$$\mathcal{T} = \{T_1, T_2, \dots, T_K\}, K \geq 2. \quad (6)$$

Note that for a simple task T_1 , we can also denote it as $\mathcal{T} = \{T_1\}$.

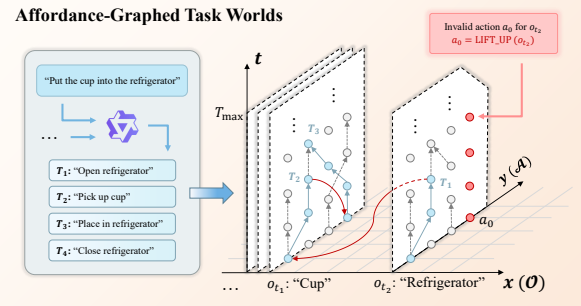


Figure 2. Affordance-Graphed Task Worlds. For any complex long-horizon task, they are decomposed into multiple simple tasks, connected via inter-task edges that bridge different object slices or reset temporal states.

Action Transfer and Joint Distribution. Unlike the intra-task action flow, the transition between two consecutive simple tasks T_k and T_{k+1} involves a semantic and physical shift, termed a *Action Transfer*. We define a action transfer

$$e_k = e\left(o_t^{(k)}, o_t^{(k+1)}\right) = \left\{a_{\text{end}}\left(o_t^{(k)}\right), a_{\text{start}}\left(o_t^{(k+1)}\right)\right\} \quad (7)$$

as the bridging operation that connects the terminal state of T_k to the initial state of T_{k+1} .

We model the joint random variables of the *Action Transfer Sequence* $\mathcal{E} = \{e_1, \dots, e_{K-1}\}$ as a conditional distribution dependent on the task decomposition $\mathcal{T} = \{T_k\}_{k=1}^K$ with

$$\mathcal{E} \sim p_{\mathcal{T}}(\mathcal{E} \mid \mathcal{T}; \epsilon_2) = \prod_{k=1}^{K-1} p_{\mathcal{T}}(e_k \mid T_k, T_{k+1}; \epsilon_2), \quad (8)$$

where ϵ_2 denotes the decomposition error introduced by the LLM when inferring the connectivity between disparate object affordances. The total probability of a successful long-horizon execution is thus the product of the success probabilities of individual simple tasks (subject to ϵ_1) and the realizability of transfer actions (subject to ϵ_2).

4. Method

In this section, we delineate our methodology AGT-World. We propose a structured modeling approach based on a *3D Semantic-Action Tensor*, transforming the task generation problem into a path planning problem within a high-dimensional sparse graph.

4.1. Task World and Compositional Reachability

To achieve generalizable task planning in any environments, we formalize the AGT-World as a universal directed graph $\mathcal{G} = (V, E)$. The vertex set V constitutes a discrete three-dimensional configuration space, which serves as an idealized, potentially infinite domain encompassing all theoretically possible object-action combinations:

$$V = \mathcal{O} \times \mathcal{A} \times \mathbb{N}^+, \quad (9)$$

where \mathcal{O} denotes the set of all theoretically manipulable objects, \mathcal{A} denotes the universal set of atomic actions, and \mathbb{N}^+ represents the discrete temporal dimension. Note that the temporal dimension denotes the relative order within a specific simple task, rather than a global absolute timestamp. And $E \subset V \times V$ represents the set of all physically or semantically feasible transitions between these configurations.

Global World State. Given a specific reconstructed scene S_0 , we instantiate a concrete *Object-Action Graph* G_{S_0} as a subgraph of \mathcal{G} . This graph is sampled from a conditional distribution dependent on the scene’s affordances:

$$G_{S_0} = (V_{S_0} = \mathcal{O}_{S_0} \times \mathcal{A}_{\text{prim}} \times \mathbb{N}^+, E_{S_0} \subset E), \quad (10)$$

where $\mathcal{O}_{S_0} \subset \mathcal{O}$ is a subset containing only objects in S_0 , and $\mathcal{A}_{\text{prim}} \subset \mathcal{A}$ is a pre-defined set of primitive actions.

We define the *Global World State* at time τ as the aggregate configuration of all objects present in the generated scene graph G_{S_0} . The state is given by:

$$S_\tau = \{s_\tau(o_i, o_j)\}_{\{o_i, o_j\} \subset \mathcal{O}_{S_0}} \subset \mathcal{S}. \quad (11)$$

This global state formulation allows us to rigorously define state transitions throughout the environment, not just for isolated objects, and S_0 is a special case when $\tau = 0$.

Graph-Based Task Representation. As illustrated in Figure 2, we model the task generation process as finding a path within G_{S_0} that satisfies a user’s high-level instruction \mathcal{I} . This path is composed of two distinct types of edges: *Intra-Task Edges* and *Inter-Task Edges*.

1. Intra-Task Edge (Action Flow): For a simple task T_k , the action flow $\pi(T_k)$ corresponds to a sequence of nodes strictly ascending the temporal dimension within the 2D slice defined by the target object $o_t^{(k)}$. These edges represent the physical execution of atomic primitives, directly altering the state S_τ .

2. Inter-Task Edge (Action Transfer): The transition between two consecutive simple tasks, T_k and T_{k+1} , is represented by an action transfer edge $e_k = e(o_t^{(k)}, o_t^{(k+1)})$. Crucially, unlike $\pi(T_k)$, the transfer edge e_k does not involve physical execution steps that consume simulation time. Instead, it represents a semantic and logical linkage-bridging the terminal action of T_k and the initial action of T_{k+1} .

To formalize this “instantaneous” context switch, we introduce the augmented state S_τ^+ . Given S_0 and a very small temporal margin $\Delta\tau > 0$, it is defined as

$$\begin{aligned} S_\tau^+ &\triangleq S_{\tau+\Delta\tau} = \{s_\tau^+(o_i, o_j)\}_{\{o_i, o_j\} \subset \mathcal{O}_{S_0}} \\ &\triangleq \{s_{\tau+\Delta\tau}(o_i, o_j)\}_{\{o_i, o_j\} \subset \mathcal{O}_{S_0}}. \end{aligned} \quad (12)$$

For a valid task decomposition, the termination of task T_k and the initialization of T_{k+1} must satisfy the boundary

condition $S_{\text{init}}^{(k+1)} = S_{\text{goal}}^{(k)+}$. Consequently, we can define the probability of a successful action transfer as:

$$\mathbb{P}(S_{\text{init}}^{(k+1)} | S_{\text{goal}}^{(k)}, e_k) = \mathbb{P}(S_{\text{goal}}^{(k)+} | S_{\text{goal}}^{(k)}, e_k) > 0. \quad (13)$$

This probability quantifies the likelihood of successfully establishing a logical connection between the $o_t^{(k)}$ and $o_t^{(k+1)}$, which is equivalent to the success probability of the LLM's high-level task decomposition, see Appendix B.

Compositional Reachability. Based on this probabilistic graph model, we provide a theoretical guarantee for the solvability of generated tasks.

Proposition 4.1 (Global Reachability via Hierarchical Composition). *Let $S_\tau \subset \mathcal{S}$ denote the global world state at time τ . Assume the AGT-World graph $G_{S_0} \subset \mathcal{G}$ satisfies:*

1. **Primitive Completeness:** For any simple task $T = \langle o_t, o_{s_1}, o_{s_2}, s_{\text{init}}, s_{\text{goal}} \rangle, s_{\text{init}}, s_{\text{goal}} \in \mathcal{S}$, there exists an action flow $\pi(T) \subset V_{S_0}$ s.t. $\mathbb{P}(s_{\text{goal}} | s_{\text{init}}, \pi) > 0$;
2. **Connectivity of Context:** For any two consecutive simple tasks T_k, T_{k+1} , if their boundary conditions align (i.e., $S_{\text{goal}}^{(k)} \approx S_{\text{init}}^{(k+1)}$), there exists an action transfer $e_k(o_t^{(k)}, o_t^{(k+1)}) \subset V_{S_0}$ connecting them with a positive probability $\mathbb{P}(S_{\text{init}}^{(k+1)} = S_{\text{goal}}^{(k)+} | S_{\text{goal}}^{(k)}, e_k) > 0$.

Then for any complex long-horizon task $\mathcal{T} = \{T_k\}_{k=1}^K$ and global world state $S_0 = S_{\text{init}}^{(1)}, S_\tau = S_{\text{goal}}^{(K)} \subset \mathcal{S}$, there exists

$$\begin{aligned} \Pi &= \{\pi_k \subset V_{S_0} : \pi_k \sim p_F(\pi | \mathcal{T}; \epsilon_1)\}_{k=1}^K, \\ \mathcal{E} &= \{e_k \subset V_{S_0} : e_k \sim p_T(e | \mathcal{T}; \epsilon_2)\}_{k=1}^{K-1}, \end{aligned}$$

such that

$$\begin{aligned} &\mathbb{P}(S_\tau | S_0, \Pi, \mathcal{E}) \\ &= \prod_{k=1}^K \underbrace{\mathbb{P}(S_{\tau_k} | S_{\tau_{k-1}}^+, \pi_k)}_{\text{Execution Feasibility}} \cdot \prod_{k=1}^{K-1} \underbrace{\mathbb{P}(S_{\tau_k}^+ | S_{\tau_k}, e_k)}_{\text{Transition Consistency}} > 0 \end{aligned} \quad (14)$$

with $[0, \tau] = \bigcup_{k=1}^K [\tau_{k-1}, \tau_k]$.

The proposition means that the global transition from S_0 to S_τ is feasible with non-zero probability, and the proof of this proposition is given in Appendix C.

4.2. Graph-Based Task Generation

At present, methods for robotic perception and dynamic representation generally fall into five categories: Pixel-based, Latent, 3D Particle, Keypoint, and Object-centric representations (Ai et al., 2025). While each has merits, our framework integrates visual feedback with a graph-based structure

to enable robust long-horizon planning. Specifically, we focus on the sub-task decomposition module, inspired by works that combine LLMs with Input-Output examples for task expansion (Wang et al., 2024) or fine-tune models like Qwen-2.5VL for decomposition (Sun et al., 2025).

Initialization via VLM-Driven Decomposition. As illustrated in Figure 3, the process begins with a user-provided keyword \mathcal{I} , the generated simulated scene S_0 , and the original real-world reference image X_0 . These inputs are fed into a VLM to propose a high-level plan and decompose it into atomic sub-tasks. This yields a posterior distribution over the complex task structure:

$$\mathcal{T} \sim p_G(\mathcal{T} | \mathcal{I}, S_0, X_0; \epsilon_3), \quad (15)$$

where ϵ_3 represents the planning uncertainty introduced by the VLM. Given this \mathcal{T} , and assuming the conditions of Proposition 4.1 are met, we can proceed to generate the specific action flows for each sub-task.

4.3. Self-Evolution for Task Progression

In this section, we introduce the Self-Evolution strategy and algorithm that uses VLM as a process supervisor. Figure 4 provides a complementary illustration of our work.

Self-Evolution Mechanism. For each sub-task $T_k \in \mathcal{T}$, the action flow $\pi(T_k) = \{a_1, \dots, a_n\}$ is executed, and we extract a sequence of video frames as visual feedback. Let $I \subset \{\text{Global, Head, Wrist}\}$ denote the set of camera views used, and p_2 be a hyperparameter controlling the frame sampling rate per action. If action a_j takes time t_j , we obtain the image sequence for the j -th action from view i as $X_{kj}^i = (x_{kj}^{i,1}, \dots, x_{kj}^{i,\lceil t_j/p_2 \rceil})$, where $x_{kj}^{il} \in \mathbb{R}^{H \times W \times 3}$.

The VLM analyzes these frames sequentially. To provide temporal context, we introduce a hyperparameter p_1 (look-back window). For the j -th step, the VLM observes the sequence of frames corresponding to actions $\{a_{\max(j-p_1, 1)}, \dots, a_j\}$. Let \mathbf{X}_{kj}^I denote the concatenated multi-view frames for this window as

$$\mathbf{X}_{kj}^I = \left\{ X_{k,\max(j-p_1, 1)}^i, \dots, X_{k,j}^i \right\}_{i \in I}, \quad (16)$$

and $\mathbf{X}_k^I = \left\{ \mathbf{X}_{kj}^I \right\}_{j=1}^{|\pi(T_k)|}$ denote the the complete visual observation for the sub-task. The VLM outputs a step-wise semantic critique $m_j \sim p_E(m | \mathbf{X}_{kj}^I; \epsilon_4)$, where ϵ_4 represents the uncertainty by the VLM. The collection of all step-wise critiques is $\mathbf{m} = \{m_j\}_{j=1}^{|\pi(T_k)|}$.

The final step aggregates all historical visual data \mathbf{X}_k^I , step-wise critiques \mathbf{m} , the overall task context \mathcal{T} , and the history of previous evolution iterations to propose the next iteration's policy. The evolution from iteration τ to $\tau + 1$ is

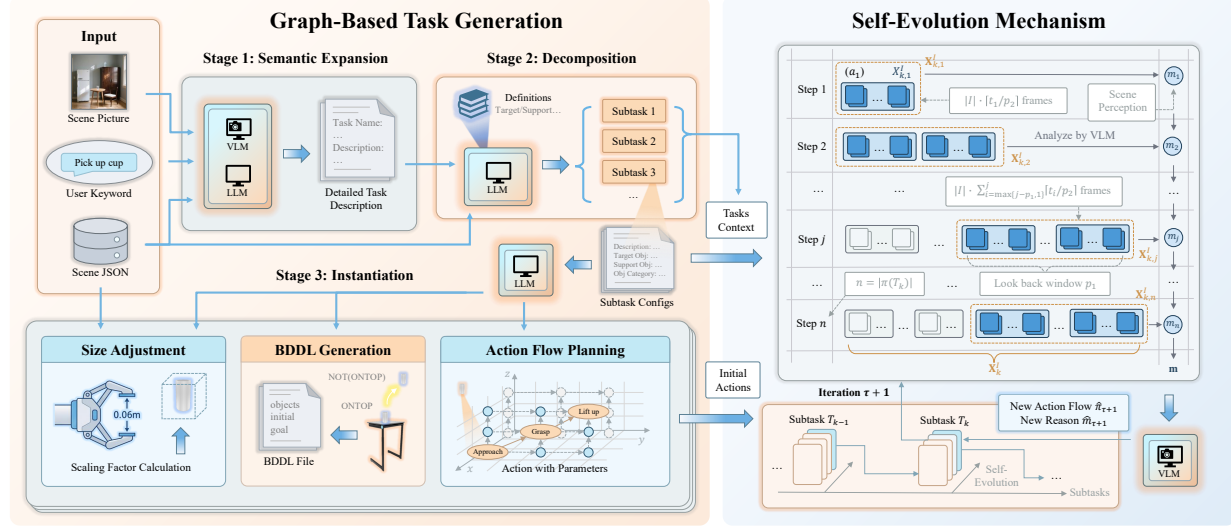


Figure 3. Graph-Based Task Generation with Self-Evolution. For the left part, **Stage I**: Received a user keyword and scene information, producing the complete task name and an expanded task-scene description. **Stage II**: Leveraging the definitions of o_t, o_{s_1}, o_{s_2} and boundary cases for decomposition, provides subtask description, and precise matching of relevant objects. **Stage III**: For each subtask, adjust target object size, generate a BDDL (Li et al., 2023) file that defines $s_{\text{init}}, s_{\text{goal}}$, and match each step with corresponding actions from the primitive action library. For the right part, we use Self-Evolution Mechanism to generate new action sequence and reasons until maximum iteration times per subtask. For details, see Appendix A.2,A.3.

modeled as:

$$(\hat{\pi}_{\tau+1}, \hat{m}_{\tau+1}) \sim p_E((\pi, m) | \mathbf{X}_k^I, \mathbf{m}, \mathcal{T}, \{(\hat{\pi}_i, \hat{m}_i)\}_{i=1}^{\tau}; \epsilon_4). \quad (17)$$

Optimization Algorithm \mathcal{A}_0 . Within the evolution step, our algorithm \mathcal{A}_0 employs two specific strategies based on the VLM’s feedback: *Sequence Modification* (correcting semantic logic errors) and *Parameter Adjustment* (fine-tuning geometric parameters). Algorithm \mathcal{A}_0 iteratively applies the sampling process described above to minimize the discrepancy between the executed and desired states.

While Proposition 4.1 assumes the existence of an optimal policy π_n within the generated graph G_{S_0} rather than the continuous universal space S . Since our action space is constructed from a finite set of discrete primitives $\mathcal{A}_{\text{prim}} \subset \mathcal{A}$ (see Appendix A.2), it cannot fully span all actions, inevitably introducing an irreducible *systematic bias* ϵ_{bias} .

5. Experiments

To test our method, we constructed large-scale scene-task pairs. In addition, we specifically designed some complex long-horizon tasks covering basic task types and conducted ablation experiments on the self-evolution mechanism.

5.1. Experimental Setup

The generated tasks categorize into three primary types: 1) Manipulation primitives such as “Open/Close” or “Pick-/Place”; 2) Transportation tasks involving mobile base navigation; and 3) Fine-grained tasks requiring precise object

positioning and stacking as “Place A inside/on B”.

Large-Scale Scene-Task Pairs. We leveraged generative models to select 34 suitable real-world scenes, and we reconstructed three interactive simulation environments for each real-world scene. This yielded **102 unique scenarios** comprising diverse scene layouts and task definitions autonomously. Here, we only test the first primary type of tasks. As shown in Table 1, our method achieves an overall success rate of **71.6%**. For all tasks results, see Figure 5 (a).

Table 1. Success Rate on 102 Tasks. This validates the reliability of our scene construction and task planning pipeline. The scene generated examples and experiment details see Appendix D.3.

Task Category	Count	Success	SR (%)
Articulated Object (Open/Close)	36	24	66.7
Rigid Object (Pick up)	66	49	74.2
Total	102	73	71.6

Representative Complex Long-Horizon Tasks. To rigorously evaluate our framework’s capabilities in handling these composite behaviors, we designed four representative complex long-horizon tasks:

- \mathcal{T}_1 : Transport a glass into a refrigerator.
- \mathcal{T}_2 : Place an apple into a refrigerator.
- \mathcal{T}_3 : Transfer an apple into a bowl.
- \mathcal{T}_4 : Place a cup onto a table.

Each complex task is a composition of the aforementioned primitive types. Because we adopted a structured task decomposition method, the actual experimental results show that the outcome of each subtask decomposition consistently remains deterministic. The details see Appendix D.4.

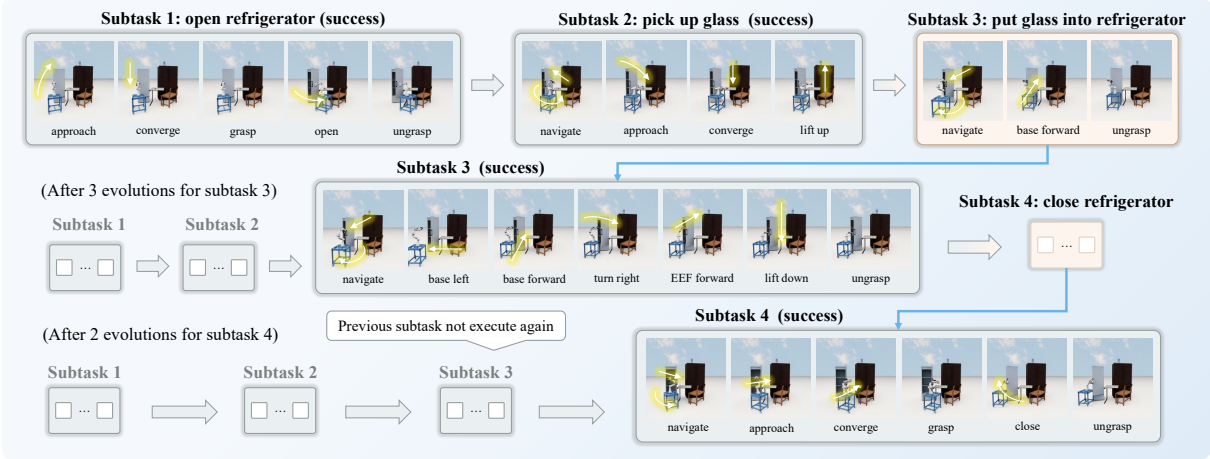


Figure 4. Detailed Action Display of Self-Evolution. Here we take the task of “Transport a glass into a refrigerator” as an example. This task is divided into four subtasks: “open refrigerator”, “pick up glass”, “put glass into refrigerator” and “close refrigerator”. Among them, subtask 3 was successfully completed after 3 iterations, while subtask 4 went through 2 iterations.

Table 2. Comparison on task diversity and feasibility. We compare with representative human-designed robotics datasets and the concurrent work. (↑) indicates higher is better for fidelity/reconstruction quality.

Metric	AGT-World	RoboGen	Behavior-100	RLBench	Meta-World	GenSim-V2	ManiSkill2
Number of Tasks	102	106	100	106	50	70	20
Task Desc. - Self-BLEU (↑)	0.806	0.284	0.299	0.317	0.322	0.378	0.674
Task Desc. - S-BERT Sim (↑)	0.376	0.165	0.210	0.200	0.263	0.288	0.194
Scene Image - ViT Sim (↑)	0.440	0.193	0.389	0.375	0.517	0.717	0.332

5.2. Task Diversity and Scene Feasibility

We evaluate the quality of our generated tasks and scenes using metrics established in prior work (Wang et al., 2024), focusing on semantic alignment and visual fidelity.

Metrics. We employ **Self-BLEU** (Papineni et al., 2002; Zhu et al., 2018) to analyze task description structure; unlike open-ended text generation, a higher score in our graph-based task generation framework indicates desirable structural consistency for robust code parsing. For semantic fidelity, we use **S-BERT** (Reimers & Gurevych, 2019; Zhu et al., 2018) to measure the alignment between user keywords and generated definitions. Finally, visual reconstruction quality is evaluated via **ViT Similarity** (Dosovitskiy et al., 2021), comparing rendered simulation images with real-world references.

Results. As shown in Table 2, our method achieves a ViT Similarity of **0.440**, outperforming many other generative baselines and comparable to human-annotated benchmarks such as Behavior-100, confirming the visual realism of our simulated scene reconstruction. Crucially, we achieve the highest S-BERT score **0.376**, demonstrating that our VLM-driven task expansion adheres strictly to user intent without hallucination. Furthermore, the high Self-BLEU score **0.860** is a deliberate outcome of our graph-based design, reflecting the highly standardized and executable program format essential for stable robot planning, contrasting with the unstructured randomness of other methods.

5.3. Task Generation and Evolution Performance

We evaluate the execution fidelity of autonomously generated tasks on four complex scenarios. For \mathcal{T}_1 and \mathcal{T}_3 , we compare Gemini-3-Flash, GPT-5.2, and the open-source model Qwen3-VL (Specifically, we all use *qwen3-vl-235b-22a-thinking*); for others, we use Qwen3-VL. We set a strict failure condition: if any sub-task exceeds 5 evolution iterations, the entire episode is marked as failed. All the results are summarized in Table 3.

Performance Analysis. Simple primitives achieve near **100%** success rates across most trials, which means the initial graph-based planning provides a solid foundation for these interactions. However, navigation-heavy subtasks or fine-grained manipulation tasks ($\mathcal{T}_1, \mathcal{T}_2, \mathcal{T}_4$ contains complex transportation tasks, $\mathcal{T}_3, \mathcal{T}_4$ need complex fine-grained manipulation), open-loop execution falters, and self-evolution becomes critical.

In \mathcal{T}_1 , Qwen3-VL achieves the best completion rate **40%** by utilizing iterations to correct placement errors, the evolutionary progression is visualized in Figure 5 (b,c). In \mathcal{T}_3 , Gemini-3-Flash excels with a **70%** success rate, achieving a high ESR **62.5%** in rescuing failed episodes. Detailed experimental results can be found in Appendix D.4,D.5. Failures in the later stages mainly stem from situations such as objects falling or getting stuck at the edges, and these situations are usually difficult to correct within a few steps. For detailed failure analysis, see Appendix D.6.

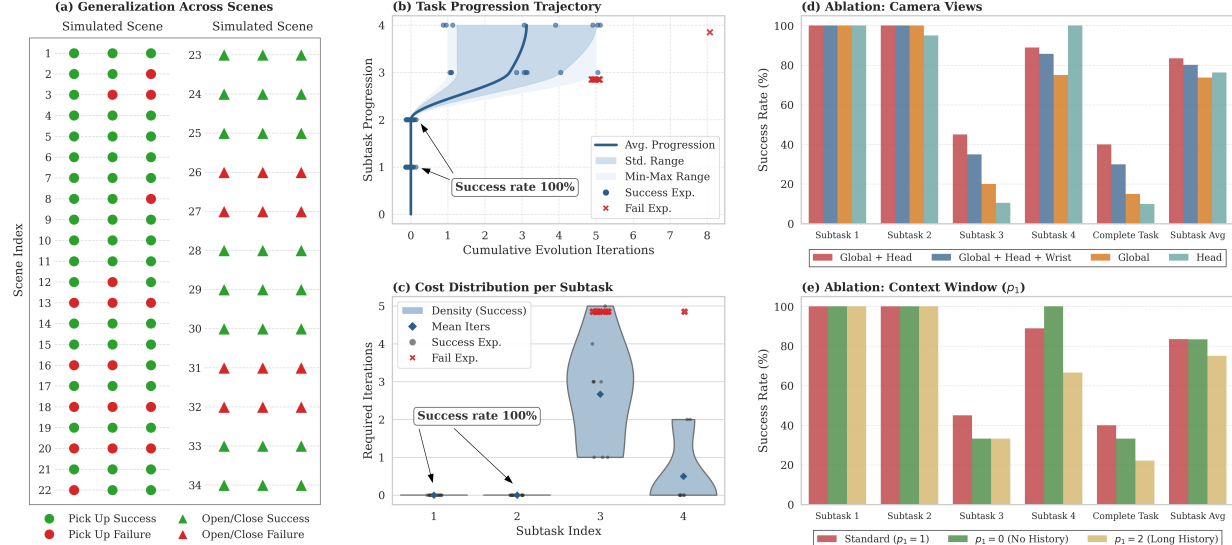


Figure 5. Comprehensive Evaluation and Ablation Studies. (a) Generalization performance across 34 diverse real-world scenes, and results are split into two type of tasks. Color indicates success (Green) or failure (Red). (b) Task progression trajectory showing the relationship between cumulative iterations and sub-task completion. (c) Cost distribution per subtask, visualizing the density of required iterations. (d) Ablation study on camera views, comparing SR across different visual input configurations. (e) Ablation study on context window (p_1), analyzing the impact of history window on SR. All ablations are performed on task T_1 using the Qwen3-VL.

Table 3. Skill Learning Performance on Long-Horizon Tasks. We report the Task Success Rate (SR, %), Evolution Success Rate (ESR, %) and Success Task Average Iterations (Iter) for each subtask stage, the complete task and subtask average.

Tasks	VLM Model	Demos	Subtask 1			Subtask 2			Subtask 3			Subtask 4			Complete Task SR	Subtask Avg SR
			SR	Iter	SR	ESR	Iter	SR	ESR	Iter	SR	ESR	Iter			
T_1 : Glass \rightarrow Fridge	Gemini-3-Flash	10	100	0	100	—	0	30	30	1.7	100	100	0.7	30	2.3	82.5 0.6
	GPT-5.2	10	100	0	100	—	0	30	30	2	66.7	66.7	1.0	20	3.5	74.2 0.8
	Qwen3-VL	20	100	0	100	—	0	45	45	2.7	88.9	66.7	0.5	40	3.1	83.5 0.8
T_2 : Apple \rightarrow Fridge	Qwen3-VL	10	100	0	100	100	0.3	40	40	1.8	75	66.7	0.7	30	2.3	78.8 0.7
T_3 : Apple \rightarrow Bowl	Gemini-3-Flash	10	100	0	70	62.5	1.6	—	—	—	—	—	—	70	1.6	92.5 0.4
	GPT-5.2	10	100	0	50	16.7	0.2	—	—	—	—	—	—	50	0.2	87.5 0.1
	Qwen3-VL	10	100	0	50	16.7	0.4	—	—	—	—	—	—	50	0.4	87.5 0.1
T_4 : Cup \rightarrow Table	Qwen3-VL	10	100	0	70	60	1.0	—	—	—	—	—	—	70	1.0	85 0.5

5.4. Ablation Studies

We conduct ablation studies to validate our design choices regarding visual feedback and temporal context.

Effect of Camera Views. We investigate the impact of the visual perspective set $I \subset \{\text{Global, Head, Wrist}\}$ provided to the VLM. As illustrated in Figure 5 (d), the standard and full view configuration achieves the similar performance, while relying solely on the Global or Head view leads to more planning failures due to limited field-of-view.

Effect of Temporal Context p_1 . We analyze the look-back window hyperparameter p_1 for the VLM’s input action history. As results in Figure 5 (e), increasing p_1 has little effect on SR while substantially increasing costs and inference latency. Therefore, we chose $p_1 = 1$ in our experiments.

6. Conclusion

In this paper, we introduced Affordance-Graphed Task Worlds (AGT-World), a unified framework that can autonomously generate physically manipulable data for scal-

able robotic learning, and also provides a theoretical framework for graph-based task generation and self-evolution. Our approach addresses the following three core challenges:

First, we bridge the semantic-physical gap by **reconstructing interactive simulated scenes** that preserve both the geometric layouts and semantic affordances of real-world observations. Second, we model the **task world as a structured graph**, enabling the precise decomposition of complex long-horizon tasks into simple tasks, which all have executable atomic actions. Third, we introduce a **self-evolution mechanism** with hybrid feedback, allowing the system to autonomously diagnose execution failures and refine policies through a closed-loop cycle of proposal, execution, and correction.

Extensive experiments demonstrate that AGT-World significantly outperforms in success rates and generalization under large-scale scene-task pairs. Furthermore, we performed well in several complex long-horizon tasks. Future work will consider combining RL strategies as agents to action categories under specific conditions, and designing pathways for sim-to-real transfer.

Impact Statement

This work presents a scalable embodied data generation method that significantly accelerates the development of general-purpose robots. Our framework lowers the barrier to training high-performance intelligent agents. By generating high-quality, long-duration demonstration data from static images, it promotes the widespread adoption of embodied artificial intelligence research.

The self-evolving mechanism directly contributes to improving the safety of robot behavior. By rigorously diagnosing and correcting failure modes in a simulated environment, our method minimizes the risk of physical damage during the early stages of learning and ensures the logical consistency of the generated policies before deployment.

We acknowledge that relying on generative foundation models may introduce biases present in the training data, and we encourage the community to utilize this process to create diverse datasets that represent various cultural and physical environments, thereby ensuring the fairness and robustness of robot generalization.

References

Ahn, M., Dwibedi, D., Finn, C., Arenas, M. G., Gopalakrishnan, K., Hausman, K., Ichter, B., Irpan, A., Joshi, N., Julian, R., et al. Autort: Embodied foundation models for large scale orchestration of robotic agents. *arXiv preprint arXiv:2401.12963*, 2024.

Ai, B., Tian, S., Shi, H., Wang, Y., Pfaff, T., Tan, C., Christensen, H. I., Su, H., Wu, J., and Li, Y. A review of learning-based dynamics models for robotic manipulation. *Science Robotics*, 10(106):eadt1497, 2025.

Bruce, J., Dennis, M. D., Edwards, A., Parker-Holder, J., Shi, Y., Hughes, E., Lai, M., Mavalankar, A., Steigewald, R., Apps, C., et al. Genie: Generative interactive environments. In *Forty-first International Conference on Machine Learning*, 2024.

Dai, T., Wong, J., Jiang, Y., Wang, C., Gokmen, C., Zhang, R., Wu, J., and Fei-Fei, L. Automated creation of digital cousins for robust policy learning. In *Conference on Robot Learning (CoRL)*, 2024.

Dosovitskiy, A., Beyer, L., Kolesnikov, A., Weissenborn, D., Zhai, X., Unterthiner, T., Dehghani, M., Minderer, M., Heigold, G., Gelly, S., Uszkoreit, J., and Houlsby, N. An image is worth 16x16 words: Transformers for image recognition at scale. In *9th International Conference on Learning Representations, ICLR 2021, Virtual Event, Austria, May 3-7, 2021*. OpenReview.net, 2021. URL <https://openreview.net/forum?id=YicbFdNTTy>.

Gan, C., Schwartz, J., Alter, S., Mrowca, D., Schrimpf, M., Traer, J., De Freitas, J., Kubilius, J., Bhandwaldar, A., Haber, N., et al. Threedworld: A platform for interactive multi-modal physical simulation. *arXiv preprint arXiv:2007.04954*, 2020.

Garrett, C. R., Mandlekar, A., Wen, B., and Fox, D. Skillmimicgen: Automated demonstration generation for efficient skill learning and deployment. In *8th Annual Conference on Robot Learning*, 2024. URL <https://openreview.net/forum?id=YOFrRTDC6d>.

Hua, P., Liu, M., Macaluso, A., Lin, Y., Zhang, W., Xu, H., and Wang, L. Gensim2: Scaling robot data generation with multi-modal and reasoning llms. In *8th Annual Conference on Robot Learning*, 2024.

Huang, H., Lin, F., Hu, Y., Wang, S., and Gao, Y. Copa: General robotic manipulation through spatial constraints of parts with foundation models. In *2024 IEEE/RSJ International Conference on Intelligent Robots and Systems (IROS)*, pp. 9488–9495. IEEE, 2024.

Kang, B., Yue, Y., Lu, R., Lin, Z., Zhao, Y., Wang, K., Huang, G., and Feng, J. How far is video generation from world model? – a physical law perspective. *arXiv preprint arXiv:2411.02385*, 2024.

Kerbl, B., Kopanas, G., Leimkühler, T., and Drettakis, G. 3d gaussian splatting for real-time radiance field rendering. *ACM Trans. Graph.*, 42(4):139–1, 2023.

Kerr, J., Kim, C. M., Goldberg, K., Kanazawa, A., and Tancik, M. Lerp: Language embedded radiance fields. In *Proceedings of the IEEE/CVF international conference on computer vision*, pp. 19729–19739, 2023.

Kim, M. J., Pertsch, K., Karamcheti, S., Xiao, T., Balakrishna, A., Nair, S., Rafailov, R., Foster, E., Lam, G., Sanketi, P., Vuong, Q., Kollar, T., Burchfiel, B., Tedrake, R., Sadigh, D., Levine, S., Liang, P., and Finn, C. Openvla: An open-source vision-language-action model, 2024. URL <https://arxiv.org/abs/2406.09246>.

Li, C., Xia, F., Martín-Martín, R., Lingelbach, M., Srivastava, S., Shen, B., Vainio, K. E., Gokmen, C., Dharan, G., Jain, T., Kurenkov, A., Liu, K., Gweon, H., Wu, J., Fei-Fei, L., and Savarese, S. igibson 2.0: Object-centric simulation for robot learning of everyday household tasks. In Faust, A., Hsu, D., and Neumann, G. (eds.), *Proceedings of the 5th Conference on Robot Learning*, volume 164 of *Proceedings of Machine Learning Research*, pp. 455–465. PMLR, 08–11 Nov 2022.

Li, C., Zhang, R., Wong, J., Gokmen, C., Srivastava, S., Martín-Martín, R., Wang, C., Levine, G., Lingelbach, M., Sun, J., et al. Behavior-1k: A benchmark for embodied ai

with 1,000 everyday activities and realistic simulation. In *Conference on Robot Learning*, pp. 80–93. PMLR, 2023.

Li, C., Xu, M., Bahety, A., Yin, H., Jiang, Y., Huang, H., Wong, J., Garlanka, S., Gokmen, C., Zhang, R., Liu, W., Wu, J., Martín-Martín, R., and Fei-Fei, L. Momagen: Generating demonstrations under soft and hard constraints for multi-step bimanual mobile manipulation, 2025a. URL <https://arxiv.org/abs/2510.18316>.

Li, D., Fang, Y., Chen, Y., Yang, S., Cao, S., Wong, J., Luo, M., Wang, X., Yin, H., Gonzalez, J. E., et al. World-modelbench: Judging video generation models as world models. *arXiv preprint arXiv:2502.20694*, 2025b.

Liao, Y., Zhou, P., Huang, S., Yang, D., Chen, S., Jiang, Y., Hu, Y., Cai, J., Liu, S., Luo, J., et al. Genie envisioner: A unified world foundation platform for robotic manipulation. *arXiv preprint arXiv:2508.05635*, 2025.

Liu, Y., Zhang, K., Li, Y., Yan, Z., Gao, C., Chen, R., Yuan, Z., Huang, Y., Sun, H., Gao, J., et al. Sora: A review on background, technology, limitations, and opportunities of large vision models. *arXiv preprint arXiv:2402.17177*, 2024.

Ma, J., Liang, W., Wang, H.-J., Zhu, Y., Fan, L., Bastani, O., and Jayaraman, D. Dreureka: Language model guided sim-to-real transfer. *Robotics: Science and Systems (RSS)*, 2024a.

Ma, Y. J., Liang, W., Wang, G., Huang, D.-A., Bastani, O., Jayaraman, D., Zhu, Y., Fan, L., and Anandkumar, A. Eureka: Human-level reward design via coding large language models. In *International Conference on Representation Learning (ICLR)*, 2024b.

Makoviychuk, V., Wawrzyniak, L., Guo, Y., Lu, M., Storey, K., Macklin, M., Hoeller, D., Rudin, N., Allshire, A., Handa, A., et al. Isaac gym: High performance gpu-based physics simulation for robot learning. *arXiv preprint arXiv:2108.10470*, 2021.

Mees, O., Ghosh, D., Pertsch, K., Black, K., Walke, H. R., Dasari, S., Hejna, J., Kreiman, T., Xu, C., Luo, J., et al. Octo: An open-source generalist robot policy. In *First Workshop on Vision-Language Models for Navigation and Manipulation at ICRA 2024*, 2024.

Meng, F., Liao, J., Tan, X., Shao, W., Lu, Q., Zhang, K., Cheng, Y., Li, D., Qiao, Y., and Luo, P. Towards world simulator: Crafting physical commonsense-based benchmark for video generation. *arXiv preprint arXiv:2410.05363*, 2024.

Nguyen, P. T., Wang, T.-H., Hong, Z.-W., Aasi, E., Silva, A., Rosman, G., Karaman, S., and Rus, D. Regen: Generative robot simulation via inverse design. In *The Thirteenth International Conference on Learning Representations*, 2025. URL <https://openreview.net/forum?id=EbCUbPZjM1>.

Quab, M., Darzet, T., Moutakanni, T., Vo, H., Szafraniec, M., Khalidov, V., Fernandez, P., Haziza, D., Massa, F., El-Nouby, A., et al. Dinov2: Learning robust visual features without supervision. *arXiv preprint arXiv:2304.07193*, 2023.

O’Neill, A., Rehman, A., Maddukuri, A., Gupta, A., Padalkar, A., Lee, A., Pooley, A., Gupta, A., Mandlekar, A., Jain, A., et al. Open x-embodiment: Robotic learning datasets and rt-x models: Open x-embodiment collaboration 0. In *2024 IEEE International Conference on Robotics and Automation (ICRA)*, pp. 6892–6903. IEEE, 2024.

Papineni, K., Roukos, S., Ward, T., and Zhu, W. J. Bleu: a method for automatic evaluation of machine translation. In *Proceedings of the 40th Annual Meeting of the Association for Computational Linguistics*, pp. 311–318, 2002. doi: 10.3115/1073083.1073135.

Radford, A., Kim, J. W., Hallacy, C., Ramesh, A., Goh, G., Agarwal, S., Sastry, G., Askell, A., Mishkin, P., Clark, J., et al. Learning transferable visual models from natural language supervision. In *International conference on machine learning*, pp. 8748–8763. PMLR, 2021.

Ravi, N., Gabeur, V., Hu, Y.-T., Hu, R., Ryali, C., Ma, T., Khedr, H., Rädle, R., Rolland, C., Gustafson, L., Mintun, E., Pan, J., Alwala, K. V., Carion, N., Wu, C.-Y., Girshick, R., Dollár, P., and Feichtenhofer, C. Sam 2: Segment anything in images and videos. *arXiv preprint arXiv:2408.00714*, 2024. URL <https://arxiv.org/abs/2408.00714>.

Reimers, N. and Gurevych, I. Sentence-bert: Sentence embeddings using siamese bert-networks. *ArXiv*, abs/1908.10084, 2019. URL <https://api.semanticscholar.org/CorpusID:201646309>.

Sun, Q., Yang, L., Tang, W., Huang, W., Xu, K., Chen, Y., Liu, M., Yang, J., Zhu, H., Wang, Y., et al. Learning primitive embodied world models: Towards scalable robotic learning. *arXiv preprint arXiv:2508.20840*, 2025.

Tao, S., Xiang, F., Shukla, A., Qin, Y., Hinrichsen, X., Yuan, X., Bao, C., Lin, X., Liu, Y., kai Chan, T., Gao, Y., Li, X., Mu, T., Xiao, N., Gurha, A., Rajesh, V. N., Choi, Y. W., Chen, Y.-R., Huang, Z., Calandra, R., Chen, R., Luo, S., and Su, H. Maniskill3: Gpu parallelized robotics

simulation and rendering for generalizable embodied ai. *Robotics: Science and Systems*, 2025.

Tian, W., Zhang, S., Zhang, K., Chi, X., Fan, C., Lu, J., Luo, Y., Zhou, Q., Zhao, Y., Liu, N., et al. Seea-r1: Tree-structured reinforcement fine-tuning for self-evolving embodied agents. *arXiv preprint arXiv:2506.21669*, 2025.

Wang, X., Liu, L., Cao, Y., Wu, R., Qin, W., Wang, D., Sui, W., and Su, Z. Embodiedgen: Towards a generative 3d world engine for embodied intelligence. *arXiv preprint arXiv:2506.10600*, 2025.

Wang, Y., Xian, Z., Chen, F., Wang, T.-H., Wang, Y., Fragkiadaki, K., Erickson, Z., Held, D., and Gan, C. Robogen: Towards unleashing infinite data for automated robot learning via generative simulation. In *Forty-first International Conference on Machine Learning*, 2024. URL <https://openreview.net/forum?id=SQID1Jd3hN>.

Yan, W., Zhang, Y., Abbeel, P., and Srinivas, A. Videogpt: Video generation using vq-vae and transformers. *arXiv preprint arXiv:2104.10157*, 2021.

Yang, L., Kang, B., Huang, Z., Zhao, Z., Xu, X., Feng, J., and Zhao, H. Depth anything v2. *Advances in Neural Information Processing Systems*, 37:21875–21911, 2024a.

Yang, Y., Sun, F.-Y., Weihs, L., VanderBilt, E., Herrasti, A., Han, W., Wu, J., Haber, N., Krishna, R., Liu, L., et al. Holodeck: Language guided generation of 3d embodied ai environments. In *Proceedings of the IEEE/CVF Conference on Computer Vision and Pattern Recognition*, pp. 16227–16237, 2024b.

Yang, Y., Gu, K., Wen, Y., Li, H., Zhao, Y., Wang, T., and Liu, X. Maniagent: An agentic framework for general robotic manipulation, 2025. URL <https://arxiv.org/abs/2510.11660>.

Yu, T., Xiao, T., Stone, A., Tompson, J., Brohan, A., Wang, S., Singh, J., Tan, C., Peralta, J., Ichter, B., et al. Scaling robot learning with semantically imagined experience. *arXiv preprint arXiv:2302.11550*, 2023.

Zhen, H., Qiu, X., Chen, P., Yang, J., Yan, X., Du, Y., Hong, Y., and Gan, C. 3d-vla: 3d vision-language-action generative world model. *arXiv preprint arXiv:2403.09631*, 2024.

Zhou, X., Qiao, Y., Xu, Z., Wang, T., Chen, Z., Zheng, J., Xiong, Z., Wang, Y., Zhang, M., Ma, P., et al. Genesis: A generative and universal physics engine for robotics and beyond. *arXiv preprint arXiv:2401.01454*, 2024.

Zhu, Y., Lu, S., Zheng, L., Guo, J., Zhang, W., Wang, J., and Yu, Y. Texxygen: A benchmarking platform for text generation models. In *The 41st International ACM SIGIR Conference on Research & Development in Information Retrieval*, pp. 1097–1100, 2018.

Zitkovich, B., Yu, T., Xu, S., Xu, P., Xiao, T., Xia, F., Wu, J., Wohlhart, P., Welker, S., Wahid, A., et al. Rt-2: Vision-language-action models transfer web knowledge to robotic control. In *Conference on Robot Learning*, pp. 2165–2183. PMLR, 2023.

Zook, A., Sun, F.-Y., Spjut, J., Blukis, V., Birchfield, S., and Tremblay, J. Grs: Generating robotic simulation tasks from real-world images. In *Proceedings of the Computer Vision and Pattern Recognition Conference*, pp. 594–603, 2025.

A. Implementation Details

A.1. Simulated Scene Generation Details

This section shows the complete process of simulated scene generation 3.1 by the reconstruction method (Dai et al., 2024). The generation of the simulation environment reconstructs an interactive simulated scene from a single real-world RGB observation, and it reserves semantic affordances and object states. The pipeline is as follows:

1. **Real-world Extraction:** Obtain data and information from the real world, input the camera's internal parameter matrix K and a single RGB image X , and output a set of object representations including object labels, masks, point clouds, etc., for the subsequent creation of simulated scenes. The main methods include observing and extracting objects (using LLM, *GroundedSAM-v2* (Ravi et al., 2024)), followed by depth estimation (*DepthAnything-v2* (Yang et al., 2024a)) and extracting point clouds, etc.
2. **Assets Matching:** Hierarchical search is conducted on the asset dataset *BEHAVIOR-1K* (Li et al., 2023). Through the *CLIP* and *DINOv2* models (Radford et al., 2021; Oquab et al., 2023), the most suitable assets are matched for each object. This step outputs the virtual assets and snapshots corresponding to each object in the corresponding direction.
3. **Simulated Scene Generation:** Improve the details such as asset location determination and scene physical stability (for example, use LLM to determine whether to install objects on the wall). And based on the *OmniGibson* platform (Li et al., 2023), simulation scenes are generated, providing physical simulation and rendering including object states, etc.

ManiAgent (Yang et al., 2025) directly estimates the 3D coordinates of real objects from RGB images using *Florence-2*, and then employs *AnyGrasp* to estimate the 6-DoF pose of the target position and plan the path. In contrast, our work estimates the 3D coordinates of each object from RGB images while reconstructing the entire simulated environment. It retains advanced scene attributes, such as spatial object layout S_0 , key semantics, and physical visibility, which offers advantages such as maintaining global physical consistency and preserving the state of complex long-horizon tasks.

A.2. Implementation Details of Graph-Based Task Generation

In this section, we provide a comprehensive breakdown of the Graph-Based Task Generation pipeline, corresponding to the left component of Figure 3 in the main paper. This process utilizes Large Language Models (LLMs) or Vision-Language Models (VLMs) to autonomously translate vague user commands into executable, physically grounded task specifications. The pipeline consists of three sequential stages: Semantic Expansion, Subtask Decomposition, and Task Instantiation.

A.2.1. SEMANTIC EXPANSION

The goal of this stage is to ground a potentially vague user query into a precise scene context.

Input:

- **User Keyword (\mathcal{I}):** This can be a specific object name (e.g., “refrigerator”, “cup”), a specific action (e.g., “pick up the cup”), or a high-level abstract instruction requiring reasoning (e.g., “put the cup in the refrigerator”, “clean the room”).
- **Scene Configuration (*scene.json*):** A JSON file containing the ground-truth metadata of the reconstructed scene, including object IDs, 3D coordinates, and bounding boxes. This is essential for grounding semantic concepts to specific simulation assets (e.g., mapping “cup” to the unique ID *glass_0*).
- **Scene Observation (Optional):** An RGB image of the scene. If provided, a VLM is employed for visual reasoning; otherwise, an LLM processes the textual JSON data.

Output:

- **Task Name (*task.name*):** A strictly formatted string where all objects are replaced by their unique scene IDs (e.g., “put *glass_0* into *cabinet_0*”).

- **Detailed Task Description (*task_message_detail*):** A step-by-step narrative of the task logic generated by the model. For example: “*This is a kitchen scene. There is a cup (glass_0) on top of a cabinet (cabinet_0). The goal is to place the cup inside the cabinet. The robot must first open the cabinet door, approach the cup, grasp it, lift it up, navigate to the cabinet, and place it inside...*

A.2.2. SUBTASK DECOMPOSITION

This stage breaks down the long-horizon task into a sequence of atomic simple tasks, bridging the definition in Section 3.2 and Section 3.3 of the main paper.

Input: The *task.name* and *task.message_detail* from A.2.1, along with the *scene.json*.

Output: A sequential list of subtask configurations (JSON). For a complex task $\mathcal{T} = \{T_1, T_2, \dots, T_K\}$, each subtask configuration contains:

- **Subtask Name:** The atomic activity (e.g., “Open Cabinet”, “Pick up Cup”).
- **Description:** Detailed instructions specific to this subtask.
- **Target Object ID (o_t):** The primary object being manipulated.
- **Support Object ID (o_{s_1}, o_{s_2}):** The two support objects are associated with the state definitions in the task: the first support object o_{s_1} specifies the initial state relative to the target object (e.g., the table supporting the cup), while the second support object o_{s_2} specifies the goal state relative to the target object (e.g., the container receiving the cup), they all extracted from the *scene.json*.
- **BDDL Category:** The specific object category mapped to the OmniGibson asset library, used for subsequent BDDL file generation.

A.2.3. SUBTASK INSTANTIATION

For each decomposed subtask, we perform three parallel instantiation steps to ensure execution feasibility: BDDL Generation, Object Size Adjustment, and Action Flow Planning.

1. BDDL Generation (Initial State and Success Detection) We utilize the Behavior Domain Definition Language (Li et al., 2023) (BDDL) to define the initial state (s_{init}) and success criteria (s_{goal}) for the simulation. The LLM generates a BDDL file based on task-specific templates.

This part inputs subtask configuration (Target/Support object categories) and outputs a standard ‘.bddl’ file. Here are some example predicates:

- s_{init} : *inroom(robot, kitchen), ontop(glass_0, table_0)*.
- s_{goal} : *open(fridge_0), inside(apple_0, bowl_0)*, or *not(ontop(cup_0, table_0))*.

2. Object Size Adjustment (Physical Feasibility) To ensure objects are graspable by the robot’s parallel gripper (maximum width $\approx 0.06\text{m}$, depending on the robot size parameters), we dynamically adjust object scales based on their bounding box extents defined in *scene.json*. We classify objects into two types:

- **Type A (Fixed/Articulated Fixtures):** Objects such as refrigerators, cabinets, microwaves, ovens, drawers, dishwashers, and tables. These are operated via handles or are static supports.
- **Type B (Manipulable Items):** Objects such as cups, glasses, apples, bottles, boxes, bowls, and knives. These must fit inside the gripper.

For type A, no scaling is applied, and return scale factor $S = 1.0$. For type B, we calculate the minimum dimension on the horizontal plane: $d_{\text{min}} = \min(\text{bbox}_x, \text{bbox}_y)$. If $d_{\text{min}} > 0.06\text{m}$, we compute a scaling factor S such that $S \times d_{\text{min}} \approx 0.05\text{m}$ (ideal grasping width). The factor S is rounded to the nearest 0.05 or 0.1 to maintain geometric consistency. Otherwise, $S = 1.0$.

3. Action Flow Planning (Primitive Library) The LLM maps the subtask description to a sequence of primitive actions. We define a library of **21 atomic primitives** in our *BasicSkill* class, covering navigation, base movement, and end-effector (EEF) manipulation.

This part inputs subtask configuration, and outputs ordered list of actions $\pi_n = \{a_1, \dots, a_n\}$, where each action is either parameter-free or parameterized.

We categorize the 21 atomic primitives based on their parameter requirements and functional domains. This categorization distinguishes between actions that rely on the underlying solver for pose determination (parameter-free) and those allowing explicit parametric tuning during the Self-Evolution phase.

3.1. Parameter-Free Context-Aware Actions.

These actions do not require explicit numerical parameters. They rely on the underlying motion planner to determine the optimal pose based on the target object's state and global ID.

- *APPROACH*: Move the End-Effector (EEF) to a pre-grasp approach pose via long-distance ballistic movement.
- *CONVERGE*: Finely align the EEF with the target handle or object centroid via short-distance precision movement.
- *GRASP*: Close the gripper to seize the target object.
- *UNGRASP*: Open the gripper to release the currently held object.
- *RETREAT*: Move the EEF away from the target to a safe retreat pose after interaction.
- *NAVIGATE_TO_TARGET*: Global navigation planner to move the robot base near the target object (o_t).
- *NAVIGATE_TO_SUPPORT*: Global navigation planner to move the robot base near the support object (o_{s_2}).

3.2. Vertical EEF Manipulation.

Controls the vertical elevation of the gripper to clear obstacles or place objects, with parameter format: `{"ID": "height_in_meters"}`.

- *LIFT_EEF_UP*: Lift the EEF vertically up.
- *LIFT_EEF_DOWN*: Move the EEF vertically down.

And moves the end-effector linearly relative to its current orientation frame, with parameter format: `{"ID": "distance_in_meters"}`.

- *MOVE_EEF_FORWARD*: Move the EEF forward.
- *MOVE_EEF_BACKWARD*: Move the EEF backward.
- *MOVE_EEF_LEFT*: Move the EEF left.
- *MOVE_EEF_RIGHT*: Move the EEF right.

3.3. Mobile Base Translation and Rotation.

Controls the linear movement of the mobile base relative to the robot's current heading, with parameter format: `{"ID": "distance_in_meters"}`.

- *MOVE_BASE_FORWARD*: Move the robotic base forward.
- *MOVE_BASE_BACKWARD*: Move the robotic base backward.
- *MOVE_BASE_LEFT*: Move the robotic base to the left (holonomic slide).

- *MOVE_BASE_RIGHT*: Move the robotic base to the right (holonomic slide).

And adjusts the robot’s orientation to face targets or navigate narrow passages, with parameter format: $\{ "ID": \text{angle_in_degrees} \}$.

- *TURN_BASE_LEFT*: Rotate the robotic base counter-clockwise.
- *TURN_BASE_RIGHT*: Rotate the robotic base clockwise.

Finally, interacts with revolute or prismatic joints (e.g., doors, drawers). The parameter defines the normalized joint positions (0.0 to 1.0) or physical limits, with parameter format: $\{ "ID": [\text{min_limit}, \text{max_limit}] \}$. We can also use *None* to use default solver limits.

- *ARTICULATE_OPEN*: Move the robotic base to open a fixture.
- *ARTICULATE_CLOSE*: Move the robotic base to close a fixture.

A.3. Implementation Details of Self-Evolution Mechanism

In this section, we detail the **Self-Evolution Mechanism** illustrated in the right panel of Figure 3. This module serves as a closed-loop feedback system that enables the agent to autonomously diagnose execution failures and refine its policy without human intervention. The implementation leverages a Vision-Language Model (VLM) (e.g., GPT-5.2, Gemini-3-Flash, or Qwen-VL) acting in two distinct roles sequentially: a *Step-wise Safety Inspector* and a *Global Task Supervisor*.

A.3.1. VISUAL DATA PRE-PROCESSING

For each atomic action a_i executed in the simulation, we capture a sequence of RGB images from multiple camera views. To optimize token usage while retaining temporal context, we apply the following pre-processing steps:

- **Multi-View Capture:** We record images from three perspectives: *Global View* (static scene overview), *Overhead View* (fixed on the robotic base), and *Wrist View* (in-hand camera). This ensures that the VLM can detect both global navigation errors and fine-grained manipulation failures.
- **Temporal Downsampling:** If an action execution generates a large number of frames, we uniformly downsample the sequence to a maximum of 6 frames.
- **Sliding Window Context:** To provide causal context, the VLM input for step t includes visual history from the previous p steps (default $p = 1$). This allows the model to assess continuity and detect error accumulation.

A.3.2. STEP-WISE SEMANTIC CRITIQUE (THE INSPECTOR)

In the first stage, the VLM operates as a **Robotic Safety Inspector**, tasked with verifying the execution fidelity of each atomic action. Formally, for the j -th action a_j in the current policy $\hat{\pi}_\tau$, the model receives the action definition and the local visual context $\mathbf{X}_{k,j}^I$ (which includes the look-back window to capture causal dynamics). The goal is to generate a step-wise semantic critique m_j that diagnoses specific execution errors.

The prompt design guides the VLM to perform three critical verification tasks. First, **Motion Verification** checks whether the robot’s physical movement aligns with the command (e.g., determining if the base successfully navigated or was physically blocked). Second, **State Contrast** involves comparing the start and end frames within the visual window to confirm state transitions, such as verifying if an object was successfully grasped versus the gripper closing on empty space. Finally, **Anomaly Detection** focuses on identifying safety violations, specifically looking for unintended collisions, such as the robotic arm striking a door, or erratic object displacements that contradict the subtask goals. The output m_j is a concise textual report summarizing these observations.

A.3.3. GLOBAL POLICY EVOLUTION (THE SUPERVISOR)

In the second stage, the VLM transitions to the role of an expert **Robotic Task Supervisor**. This module aggregates the sequence of step-wise critiques $\mathbf{m} = \{m_j\}$ along with the complete visual history \mathbf{X}_k^I to deduce the root cause of failure and propose an optimized policy $\hat{\pi}_{\tau+1}$.

The input to this stage is comprehensive, including the original action sequence, the accumulated critiques, key visual evidence (start/end states), and crucially, the **Evolution History** $\mathcal{H}_\tau = \{(\hat{\pi}_i, \hat{m}_i)\}_{i=0}^\tau$. This history log serves as a memory buffer, ensuring the model avoids repeating previously failed configurations. The prompts enforces a strict reasoning logic:

1. **Root Cause Analysis:** The model must trace the chain of events to pinpoint the exact step where the error originated, rather than just identifying the final symptom.
2. **Path Re-planning & Parameter Tuning:** Based on the diagnosis, the model generates a new plan. This may involve inserting navigation waypoints to avoid obstacles or fine-tuning parameters.
3. **Constraint Satisfaction:** The proposed sequence must be strictly composed of the valid primitives defined in Appendix A.2.

The output is a tuple $(\hat{\pi}_{\tau+1}, \hat{m}_{\tau+1})$, containing the reasoned explanation and the revised action sequence for the next iteration.

A.3.4. ALGORITHM SUMMARY

The overall Self-Evolution process is formalized in Algorithm 1.

Algorithm 1 Self-Evolution via Hybrid Feedback

```

1: Input: Initial subtask policy  $\hat{\pi}_0$ , Task Context  $\mathcal{T}$ , Max iterations  $\tau_{\max}$ 
2: Initialize evolution history  $\mathcal{H} \leftarrow \emptyset$ 
3: for  $\tau = 0$  to  $\tau_{\max}$  do
4:   Execute  $\hat{\pi}_\tau$  in simulation, capture visual frames  $\mathbf{X}_k^I$ 
5:   if Success Condition Met ( $s_{\text{goal}}$  satisfied) then
6:     Output:  $\hat{\pi}_\tau$ 
7:   end if
8:   Initialize critique vector  $\mathbf{m} \leftarrow \emptyset$ 
9:   for each action step  $j$  in  $\hat{\pi}_\tau$  do
10:    Construct sliding window context  $\mathbf{X}_{k,j}^I$ 
11:     $m_j \leftarrow \text{VLM}_{\text{Inspector}}(a_j, \mathbf{X}_{k,j}^I)$ 
12:     $\mathbf{m}.\text{append}(m_j)$ 
13:   end for
14:    $(\hat{\pi}_{\tau+1}, \hat{m}_{\tau+1}) \leftarrow \text{VLM}_{\text{Supervisor}}(\hat{\pi}_\tau, \mathbf{m}, \mathbf{X}_k^I, \mathcal{H})$ 
15:   Update history  $\mathcal{H} \leftarrow \mathcal{H} \cup \{(\hat{\pi}_\tau, \hat{m}_{\tau+1})\}$ 
16: end for
17: Output: Failure

```

B. Probabilistic Interpretation of Action Transfer via Stochastic State Switching

In this section, we provide a detailed interpretation of the probability definition presented in the action transfer mechanism. Recall the formalization of the “instantaneous” context switch via the augmented state S_τ^+ . Given S_0 and a very small temporal margin $\Delta\tau > 0$, it is defined as:

$$\begin{aligned}
S_\tau^+ &\triangleq S_{\tau+\Delta\tau} = \{s_\tau^+(o_i, o_j)\}_{\{o_i, o_j\} \subset \mathcal{O}_{S_0}} \\
&\triangleq \{s_{\tau+\Delta\tau}(o_i, o_j)\}_{\{o_i, o_j\} \subset \mathcal{O}_{S_0}}.
\end{aligned} \tag{18}$$

For a valid task decomposition, the termination of task T_k and the initialization of T_{k+1} must satisfy the boundary condition $S_{\text{init}}^{(k+1)} = S_{\text{goal}}^{(k)+}$. Consequently, we define the probability of a successful action transfer as:

$$\mathbb{P}\left(S_{\text{init}}^{(k+1)} \mid S_{\text{goal}}^{(k)}, e_k\right) = \mathbb{P}\left(S_{\text{goal}}^{(k)+} \mid S_{\text{goal}}^{(k)}, e_k\right) > 0. \quad (19)$$

This probability quantifies the likelihood of successfully establishing a logical connection between $o_t^{(k)}$ and $o_t^{(k+1)}$, which is equivalent to the success probability of the LLM’s high-level task decomposition.

1. The Paradox of Physical Continuity

A natural question arises regarding the value of this probability. In a physically consistent simulation, as the temporal margin $\Delta\tau \rightarrow 0$, the physical state of the world remains continuous. Specifically, for stable global states (e.g., objects resting on tables), $S_{\text{goal}}^{(k)}$ is numerically nearly identical to $S_{\text{goal}}^{(k)+}$. One might therefore assume that the transition probability should strictly be 1.

However, in the AGT-WorlD framework, S_τ represents not just a snapshot of coordinates, but a set of state functions governed by specific task dynamics. The probability $\mathbb{P}(\cdot \mid \cdot, e_k)$ measures the feasibility of **Functional Switching** rather than just kinematic continuity, which change the underlying stochastic processes governing the objects.

2. Stochastic Functional Switching

To elucidate this, let us assume the total task sequence $\mathcal{T} = \{T_k\}_{k=1}^K$ corresponds to the execution time $[0, \tau] = \bigcup_{k=1}^K [\tau_{k-1}, \tau_k]$. Consider the boundary between T_k and T_{k+1} . Without loss of generality, assume this transition involves a switch in the target object from $o_t^{(k)}$ to $o_t^{(k+1)}$ and $o_t^{(k)} \neq o_t^{(k+1)}$.

Phase 1: Invariance During T_k . Consider the object relations relevant to the next task T_{k+1} , specifically the states involving its target $o_t^{(k+1)}$ and its supports $\{o_{s_1}^{(k+1)}, o_{s_2}^{(k+1)}\}$. Let us assume for this analysis that $o_t^{(k+1)}$ is not involved in the active manipulation of T_k (i.e., it is neither the target $o_t^{(k)}$ nor a support). During the time interval $[\tau_{k-1}, \tau_k]$, the states $s(o_t^{(k+1)}, o_{s_1}^{(k+1)})$ and $s(o_t^{(k+1)}, o_{s_2}^{(k+1)})$ are governed by an identity function (background invariance). They are effectively **constants**:

$$\forall \tau \in [\tau_{k-1}, \tau_k], \quad s_\tau(o_t^{(k+1)}, \cdot) = \text{Const.} \quad (20)$$

Phase 2: Activation During T_{k+1} . Upon the activation of transfer e_k at $\tau = \tau_k$, the context switches. For the duration of T_{k+1} (starting at $\tau_k + \Delta\tau$), these same state variables $s(o_t^{(k+1)}, o_{s_1}^{(k+1)})$ and $s(o_t^{(k+1)}, o_{s_2}^{(k+1)})$ cease to be constants. They become **Time-Dependent Random Variables** determined by the new action flow π_{k+1} and the associated stopping times δ :

- Initialization Release:** The state $s(o_t^{(k+1)}, o_{s_1}^{(k+1)})$ transitions from its initial configuration to a transient state at time $\tau_k + \Delta\tau + \delta_1$, where δ_1 is a random variable $0 < \delta_1 < \tau_{k+1} - (\tau_k + \Delta\tau)$.
- Goal Achievement:** The state $s(o_t^{(k+1)}, o_{s_2}^{(k+1)})$ transitions to the success criteria s_{goal} at time $\tau_k + \Delta\tau + \delta_2$, where δ_2 is a random variable $0 < \delta_2 < \tau_{k+1} - (\tau_k + \Delta\tau)$.

The Role of Transfer Probability. The transition $S_{\text{goal}}^{(k)} \xrightarrow{e_k} S_{\text{goal}}^{(k)+}$ represents the instantaneous switch from the “Constant” regime to the “Stochastic Process” regime. Although the numerical values of the states may be identical at the boundary, the *definition* of the variables changes fundamental types. The probability $\mathbb{P} > 0$ asserts that this semantic switch is valid—i.e., that the object $o_t^{(k+1)}$ is in a valid condition to accept the assignment of the new stochastic functions defined by δ_1 and δ_2 .

3. Generalization to Overlapping Contexts

The logic above holds even when object indices overlap. For instance, if $o_t^{(k)} = o_t^{(k+1)}$ (e.g., picking up an object and then immediately placing it), the governing dynamics still change. In T_k , the state $s(o_t, o_{s_2})$ might represent a “to-be-reached” condition. In T_{k+1} , that same relationship might become a “pre-condition” or “to-be-released” condition. Since the task tuple $\langle o_t, o_{s_1}, o_{s_2} \rangle$ changes at least one element or the definition of s_{goal} , the functional dependency on time δ changes signature.

Therefore, the action transfer probability serves as a semantic gatekeeper. It ensures that the Global World State can validly transition from one set of active affordance functions to another, reflecting the logical consistency of the task graph generated by the VLM.

C. Proof of Proposition 4.1

In this section, we provide the detailed proof for Proposition 4.1, demonstrating that the *AGT-World* framework guarantees the feasibility of complex long-horizon tasks through hierarchical composition.

Proof. The proof proceeds by first establishing the existence of local solutions for each atomic segment via spatial decomposition (Step 1), and then aggregating these segments into a global trajectory using the temporal chain rule (Step 2).

1. Spatial Decomposition into Object-Centric States

We first analyze the feasibility of individual components within the task sequence. The global world state S_τ is defined as the set of all object pair states in the scene: $S_\tau = \{s_\tau(o_i, o_j)\}_{\{o_i, o_j\} \subset \mathcal{O}_{S_0}}$.

Unlike a monolithic state transition, the action flow $\pi(T_k)$ of a simple task T_k only operates on specific objects defined in the tuple $T_k = \langle o_t^{(k)}, o_{s_1}^{(k)}, o_{s_2}^{(k)}, s_{\text{init}}, s_{\text{goal}} \rangle$. Consequently, we analyze the transition probability by decomposing the global state into involved and uninvolvolved object pairs.

Part A: Execution Feasibility via Intra-Task Scope

Consider the execution phase of the k -th simple task, transforming the state from $S_{\tau_{k-1}}^+$ to S_{τ_k} . The action flow π_k acts exclusively on the target object $o_t^{(k)}$ relative to its supports.

The global state change is restricted to the relationships between the target $o_t^{(k)}$ and its initial support $o_{s_1}^{(k)}$, and between $o_t^{(k)}$ and its goal support $o_{s_2}^{(k)}$. Specifically, let $\Delta\tau > 0$ be the small transfer margin. The state changes occur at specific relative time steps within the execution window $[\tau_{k-1} + \Delta\tau, \tau_k]$:

- Initialization Release:** The state $s(o_t^{(k)}, o_{s_1}^{(k)})$ transitions from its initial configuration to a transient state at time $\tau_{k-1} + \Delta\tau + \delta_1$, where $0 < \delta_1 < \tau_k - (\tau_{k-1} + \Delta\tau)$.
- Goal Achievement:** The state $s(o_t^{(k)}, o_{s_2}^{(k)})$ transitions to the success criteria s_{goal} at time $\tau_{k-1} + \Delta\tau + \delta_2$, where $0 < \delta_2 < \tau_k - (\tau_{k-1} + \Delta\tau)$.

For all other object pairs $\{o_i, o_j\}$ that are not subsets of $\{o_t^{(k)}, o_{s_1}^{(k)}, o_{s_2}^{(k)}\}$, the action flow π_k implies an identity transformation (state invariance). Thus, for the global world state S_τ where $\tau_{k-1} + \Delta\tau < \tau \leq \tau_k$:

$$\forall \{o_i, o_j\} \not\subset \{o_t^{(k)}, o_{s_1}^{(k)}, o_{s_2}^{(k)}\}, \quad \mathbb{P}(s_{\tau_k}(o_i, o_j) = s_{\tau_{k-1}}^+(o_i, o_j) \mid S_{\tau_{k-1}}^+, \pi_k) = 1. \quad (21)$$

By the **Primitive Completeness** assumption in Proposition 4.1, for the specific target and support objects involved in T_k , there exists an optimal policy π_k such that the specific transition from s_{init} to s_{goal} occurs with positive probability. Since the global transition probability is the joint probability of all constituent object states (intersection of local successes and invariances), and the intersection of events with probability 1 and positive probability is positive, we obtain:

$$\mathbb{P}(S_{\tau_k} \mid S_{\tau_{k-1}}^+, \pi_k) > 0. \quad (22)$$

This confirms that a valid action flow π_k exists for each subtask T_k .

Part B: Transition Consistency via Connectivity

We next consider the transition from the post-execution state S_{τ_k} of task T_k to the pre-execution state $S_{\tau_k}^+$ of task T_{k+1} . This corresponds to the semantic logic shift facilitated by the transfer action e_k .

Similar to Part A, this transition is instantaneous in simulation time (or occurs within margin $\Delta\tau$) and represents a re-indexing of context. By the **Connectivity of Context** assumption, the boundary conditions of consecutive tasks align, i.e., $S_{\text{goal}}^{(k)} \approx S_{\text{init}}^{(k+1)}$.

This alignment implies that there exists a valid decomposition by the VLM such that the logical link e_k bridges the two subtasks. Consequently, the probability of successfully shifting the global context is non-zero:

$$\mathbb{P}\left(S_{\text{init}}^{(k+1)} = S_{\text{goal}}^{(k)} \mid S_{\text{goal}}^{(k)}, e_k\right) > 0. \quad (23)$$

This guarantees the existence of the transfer edge $e_k \in \mathcal{E}$.

Remark on Temporal Allocation. Ideally, the total task duration is the union of subtask intervals $[0, \tau] = \bigcup_{k=1}^K [\tau_{k-1}, \tau_k]$. In our generative modeling, τ and the specific timestamps δ are treated as random variables within the idealized configuration space. Since we have established the spatial and semantic feasibility, there exists a valid temporal scaling (robot execution speed) that satisfies the sequence constraints. We therefore assume the temporal assignment is solvable without loss of generality.

2. Temporal Decomposition via Chain Rule and Markov Property

Having established the existence of valid local transitions π_k and e_k for all k , we now construct the global trajectory probability. Let the global execution trajectory be represented as a directed sequence of state transitions:

$$S_0 \xrightarrow{\pi_1} S_{\tau_1} \xrightarrow{e_1} S_{\tau_1}^+ \xrightarrow{\pi_2} S_{\tau_2} \dots \xrightarrow{e_{K-1}} S_{\tau_{K-1}}^+ \xrightarrow{\pi_K} S_{\tau_K}. \quad (24)$$

We aim to compute the conditional probability of reaching the final state $S_\tau = S_{\tau_K}$ given the initial state S_0 . Based on the analysis in Step 1, we identify the set of action flows and transfer edges:

$$\Pi = \{\pi_k \subset V_{S_0} : \pi_k \sim p_F(\pi \mid \mathcal{T}; \epsilon_1)\}_{k=1}^K, \quad (25)$$

$$\mathcal{E} = \{e_k \subset V_{S_0} : e_k \sim p_T(e \mid \mathcal{T}; \epsilon_2)\}_{k=1}^{K-1}. \quad (26)$$

By applying the *Chain Rule of Probability* and invoking the *Markov Property* inherent in the AGT-World graph structure (where S_{τ_k} depends only on $S_{\tau_{k-1}}^+$, π_k , and $S_{\tau_k}^+$ depends only on S_{τ_k} , e_k), the joint probability of the trajectory is:

$$\mathbb{P}(S_\tau \mid S_0, \Pi, \mathcal{E}) = \prod_{k=1}^K \underbrace{\mathbb{P}(S_{\tau_k} \mid S_{\tau_{k-1}}^+, \pi_k)}_{\text{Part A: } >0} \cdot \prod_{k=1}^{K-1} \underbrace{\mathbb{P}(S_{\tau_k}^+ \mid S_{\tau_k}, e_k)}_{\text{Part B: } >0}. \quad (27)$$

3. Conclusion

From Step 1, we proved that for every k , the execution probability $\mathbb{P}(S_{\tau_k} \mid S_{\tau_{k-1}}^+, \pi_k)$ is strictly positive due to primitive completeness and object-centric invariance. Similarly, the transition probability $\mathbb{P}(S_{\tau_k}^+ \mid S_{\tau_k}, e_k)$ is strictly positive due to context connectivity.

Since the product of a finite sequence of strictly positive real numbers is strictly positive, we conclude:

$$\mathbb{P}(S_\tau \mid S_0, \Pi, \mathcal{E}) > 0. \quad (28)$$

This confirms that there exists a valid decomposition consisting of policy sequence Π and transfer sequence \mathcal{E} such that the global transition from S_0 to S_τ is feasible. \square

D. More experimental results

D.1. The Details of Three Camera View

In our Self-Evolution mechanism, the VLM receives visual feedback from a set of cameras $I \subset \{\text{Global, Head, Wrist}\}$. Each perspective offers distinct information density and spatial context, contributing differently to the planning and verification process.

1. **Global View (Static Scene Overview):** This view corresponds to the original perspective of the real-world input image. Since real-world photos lack intrinsic camera parameter matrices, we estimate these parameters during the simulated scene reconstruction process to align the simulation camera with the original photo's pose. This view provides the most comprehensive understanding of the task execution, capturing the relative positions of the robot, the target object, and the support surface simultaneously. It is the primary source for checking task completion logic.

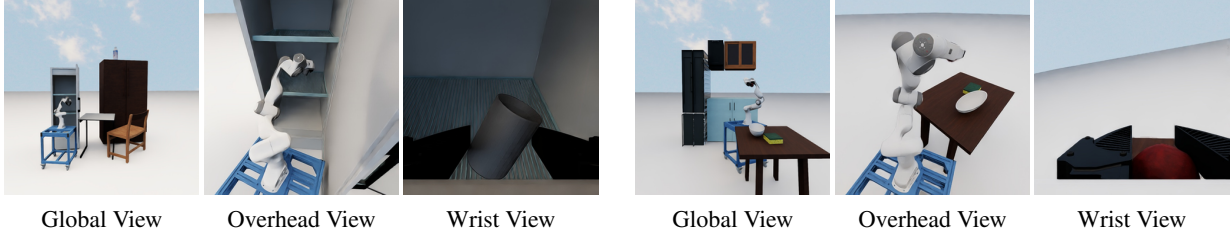


Figure 6. Visual Comparison of Camera Perspectives. The figure is divided into two task scenarios. **Left (Columns 1-3):** The task “Put the cup into the refrigerator”. The *Global View* reveals the arm reaching inside the fridge, though the specific arm posture is occluded. The *Overhead View* clearly shows the robot’s joint state and the open fridge door. The *Wrist View* captures the close-up of the cup within the gripper. **Right (Columns 4-6):** The task “Place the apple into the bowl”. The *Global View* shows the overall layout, but depth ambiguity makes it hard to judge if the apple is perfectly over the bowl. The *Overhead View* compensates for this by showing the alignment relative to the base. However, since the gripper is in mid-air, the *Wrist View* captures mostly empty space, providing little actionable information.

2. **Overhead View (Robot-Following):** This camera is mounted virtually above the mobile base and moves synchronously with the robot. It serves as an approximation of a “third-person” view bound to the agent. This perspective allows for clear observation of the robotic arm’s pose, joint configurations, and gripper status (open/closed). However, it lacks global environmental context. As shown in our ablation study Figure 5 (d), relying solely on this view degrades performance in tasks requiring affordance reasoning—for example, it is often impossible to determine the opening direction of a refrigerator door from this angle, leading to navigation failures.
3. **Wrist View (End-Effector Camera):** Fixed to the robotic arm’s wrist, this camera looks directly at the gripper’s target. Its field of view is extremely limited, capturing only the immediate interaction area. While theoretically useful for fine-grained verification (e.g., checking if a cup is level), it offers almost no utility for the coarse trajectory planning and semantic reasoning required in our graph-based generation. Consequently, as indicated in Figure 5 (d), adding this view provides negligible performance gains for our task, as the global and overhead views provide sufficient information.

D.2. Robot System and Execution Details

Robot Configuration and Control. We employ a *Franka*¹ mounted robotic arm equipped with a mobile base for all experiments. The agent perceives the environment through on-board RGB-D sensors. Motion planning is governed by an **Inverse Kinematics (IK)** controller. For each primitive action defined in the graph, the system first calculates the target coordinate and pose for either the mobile base or the End-Effector (EEF). The IK controller then generates a continuous motion path to reach these targets sequentially. To ensure safe interaction, we initialize the robot at a fixed offset distance relative to the target object before the start of any task execution.

Scale Adaptation. A challenge inherent to monocular 3D reconstruction is the ambiguity of absolute scale. Since the scene dimensions are estimated from a single image, the physical size of the reconstructed environment may vary from real-world norms. This discrepancy necessitates a rescaling of the robotic agent to match the simulation’s affordances. Through empirical testing, we uniformly set the robot scale factor to $s = 0.7$. While this setting works for the majority of our generated scenes, we observed a few failure cases still stemming from scale mismatch.

Grasping Hyperparameters. The precision of the *CONVERGE* primitive, which moves the gripper to the final grasping position, is highly sensitive to the distance offset parameter. This offset dictates how far the gripper stops in front of the target coordinate.

If the offset is set too low, the gripper extends too far forward. For tasks like “Pick up object from table”, this often causes the gripper to collide with the object or grasp it too high, leading to instability. If the offset is set too high, the gripper may stop prematurely, resulting in “grasping air” failure where the fingers close without contacting the object.

To address this, we define the convergence offset as a function of the robot’s scale. In our experiments, we use a unified hyperparameter: $\delta_{\text{offset}} = 0.14 \times s$, where $s = 0.7$. This adaptive value ensures that the gripper positioning remains consistent relative to the scaled robot body.

D.3. Scalable Scene Generation Statistics

In this section, we provide detailed statistics on the dataset construction, visualize the generated environments, and evaluate the success rates of the autonomously generated atomic tasks.

To ensure the diversity and realism of our evaluation environment, we constructed a dataset of **102 unique interactive scenarios**. The generation process follows a hierarchical pipeline:

1. **Source Image Generation:** We utilized *Qwen3-Max* and *Seedream4.5*, a state-of-the-art generative model, to synthesize 34 high-quality real-world reference images. To cover the most common household manipulation settings, we prompted the model to generate diverse layouts. The distribution includes:
 - **16 Kitchens:** Focusing on complex articulated objects like refrigerators, ovens, microwaves, and cabinets.
 - **10 Bedrooms:** Focusing on wardrobes, drawers, and bedside tables.
 - **8 Others (Study Rooms, Workshops, etc.):** Focusing on tables, shelves, and miscellaneous clutter.
2. **Simulated Scene Reconstruction:** Using the reconstruction pipeline (Dai et al., 2024), we extracted semantic and geometric information from these 34 images.
3. **Variation Augmentation:** To further expand the dataset, we generated **3 unique variations** for each real-world reference by randomizing the top-3 matched assets from the BEHAVIOR-1K dataset (e.g., matching a “fridge” in the image to three different interactive fridge models in simulation). This resulted in a total of $34 \times 3 = 102$ simulation environments.

Automated Task Proposal.

Unlike manual task design, our framework leverages the **Graph-Based Task Generation** module (detailed in Appendix A.2) to autonomously populate these scenes with valid tasks.

For each of the 102 scenes, we employ a VLM to analyze the spatial layout and propose a context-aware keyword (e.g., “cup”, “open fridge”). The system then expands this keyword into a full task definition tuple `(task_name, task_message)`. This automated pipeline ensures that the generated tasks are not only semantically aligned with the visual scene but also grounded in the available physical assets. Consequently, we obtained 102 distinct *Scene-Task Pairs*, serving as a reliable benchmark for evaluating the robustness of our method.

Visualization of Simulated Scene.

We visualize a subset of the generated pairs in Figure 7. The top row displays the reference real-world images generated by *Qwen3-Max* or *Seedream-4.5*, while the bottom row shows the reconstructed interactive simulated scenes in OmniGibson. Despite the domain gap, our framework successfully preserves the semantic layout (e.g., the relative position of the fridge and table) and functional affordances (e.g., the graspability of handles), providing a solid foundation for task execution.

Evaluation of Atomic Task Generation.

To validate the effectiveness of our Graph-Based Task Generation mechanism, we evaluated the execution success rate on the 102 generated Scene-Task pairs.

Since the primary goal here is to assess the feasibility of the generated tasks and the robustness of the graph-based planner, these tasks are primarily **Simple Tasks** (atomic primitives) such as “Open Refrigerator” or “Pick up Cup”. For this experiment, we disabled the *Self-Evolution* mechanism and relied solely on the initial open-loop plan generated by the graph solver.

As shown in Table 1, our method achieves an overall success rate of **71.6%** across 102 tasks. By analyzing our experimental results, the following conclusions can be drawn:

- **Feasibility:** The high success rate confirms that our reconstruction method and affordance-graph planning effectively bridge the sim-to-real gap, producing physically feasible task definitions.
- **Efficiency:** This result demonstrates that AGT-WorlD can serve as a low-cost, high-throughput engine for generating large-scale, high-quality demonstration data without human annotation.

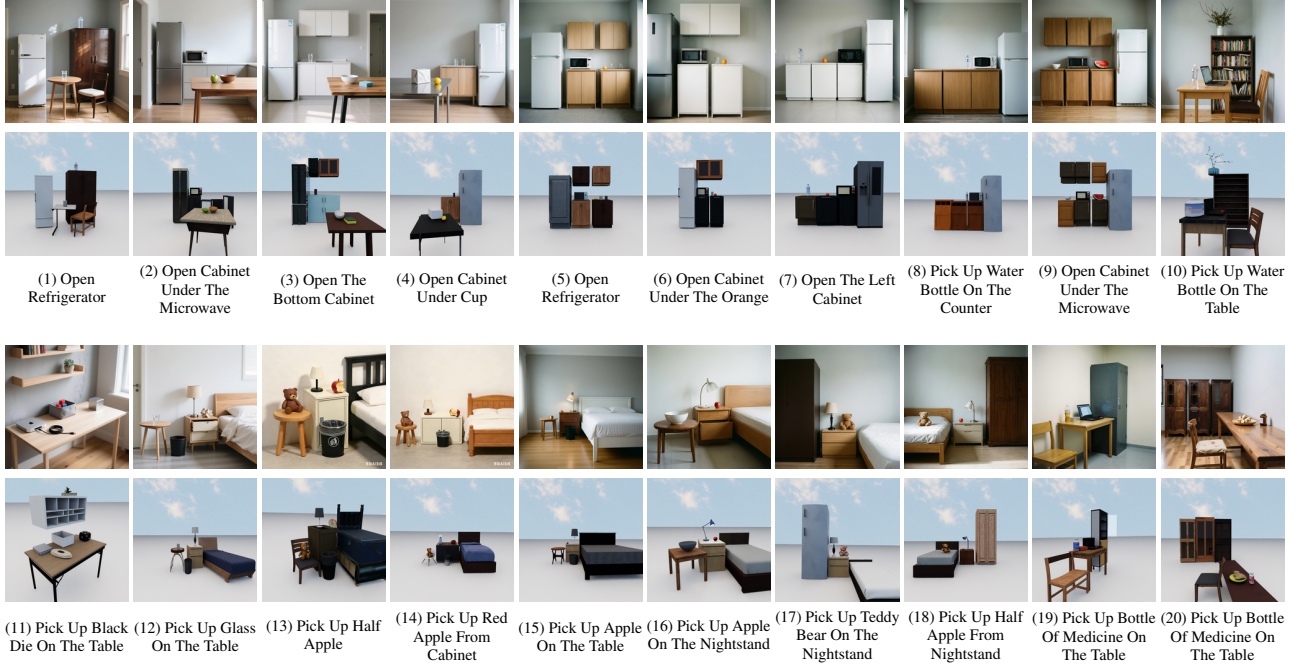


Figure 7. Visualization of 20 Representative Scene-Task Pairs. **Top Row:** Real-world reference images generated by Qwen3-Max or Seedream-4.5. **Bottom Row:** Reconstructed interactive simulation environments. Each column corresponds to a specific atomic task proposed by the VLM, demonstrating our framework’s ability to generate diverse household scenarios.

- **Role of Self-Evolution:** The failure cases (approx. 28.4%) were mostly due to edge cases (e.g., kinematic singularities in very narrow corners). This justifies our framework’s design: using the efficient Graph-Based generator for the vast majority of data production, while reserving the computationally more expensive *Self-Evolution* mechanism (Section 4.3) as a specialized agent to solve complex, long-horizon, or failure-prone edge cases.

D.4. Performance of Example Complex Long-Horizon Tasks

In this section, we provide a granular breakdown of the generation and instantiation process for the four representative complex long-horizon tasks (\mathcal{T}_1 to \mathcal{T}_4). We detail the intermediate outputs of our pipeline, from semantic expansion to action flow planning, to demonstrate the reliability and logical consistency of AGT-WorlD.

D.4.1. VISUAL OVERVIEW OF EXAMPLES SCENARIOS

To intuitively present the experimental setup, Figure 8 visualizes the four tasks using a structured grid. Each complex long-horizon task will display real-world picture, simulated reconstruction scene, main target object, main support object, and the user keyword.

D.4.2. SEMANTIC EXPANSION RESULTS

Upon receiving the user keyword, scene configuration, and observation, the VLM performs Semantic Expansion. While the exact phrasing may vary slightly across different demo runs due to the probabilistic nature of VLMs, the semantic intent remains strictly consistent with the user’s instructions. The following are representative outputs for a single demo of each complex long-horizon task:

\mathcal{T}_1 : Transport a glass into a refrigerator.

```
"task_activity_name": "open_the_refrigerator_and_put_the_glass_into_the_refrigerator",
",
"task_detail_message": "This is a kitchen scene, and there is a glass_0 on the
table_0, and there is a refrigerator_0 on the left side. The task we need to
```

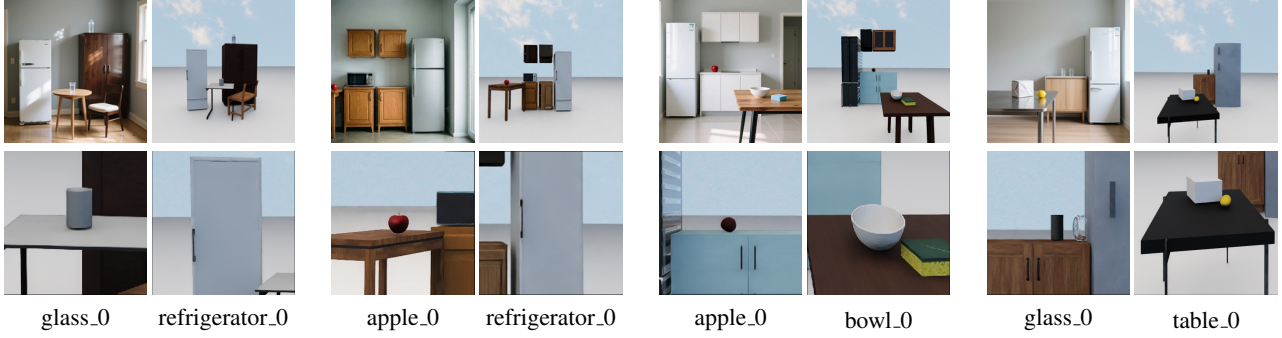


Figure 8. Visual Overview of Complex Long-Horizon Tasks. **Row 1:** Pairs of real-world reference images and reconstructed simulation environments. **Row 2:** Close-up views of the main target object and support object matched from the simulation environments. **Row 3:** The user-provided keywords that seed the autonomous task generation process.

accomplish is to put the `glass_0` on the `table_0` into the `refrigerator_0`. The robot needs to perform a sequence of actions. First, the robotic arm needs to approach the handle of the `refrigerator_0` and rotate to open it. Second, pick up the `glass_0` from the `table_0` and place it inside the `refrigerator_0`. Finally, close the `refrigerator_0`."

\mathcal{T}_2 : Place an apple into a refrigerator.

```
"task_activity_name": "open_the_refrigerator_and_put_the_apple_into_the_refrigerator",
",
"task_detail_message": "This is a modern kitchen scene. The initial condition is that there is a half_apple (apple_0) resting on top of a breakfast_table (table_0), and a refrigerator (refrigerator_0) is positioned to the right side of the scene, mounted against the wall. The task we need to accomplish is to put the apple_0 into the refrigerator_0. The robot needs to perform a sequence of actions: First, approach the refrigerator_0 and open its door by grasping and rotating the handle. Second, pick up the apple_0 from the table_0. Third, carefully place the apple_0 inside the refrigerator_0. Finally, close the refrigerator_0 door to complete the task."
```

\mathcal{T}_3 : Transfer an apple into a bowl.

```
"task_activity_name": "pick_up_apple_and_put_into_bowl",
"task_detail_message": "This is a modern kitchen scene. The initial condition is that there is an apple_0 resting on the countertop of cabinet_0, and a bowl_0 placed on the wooden table_0 in the foreground. The task we need to accomplish is to pick up the apple_0 from the countertop and place it into the bowl_0. The robotic arm must first approach and grasp the apple_0 while it is stationary on the cabinet_0 surface. Then, without releasing the apple_0, the arm must move it over to the bowl_0 on the table_0 and gently release it inside the bowl_0. No container needs to be opened or closed as both objects are accessible and unobstructed."
```

\mathcal{T}_4 : Place a cup onto a table.

```

"task_activity_name": "put_the_glass_on_the_table",
"task_detail_message": "This is a modern kitchen scene. The initial condition is
    that there is a glass_0 (water_glass) currently located near the cabinet_0, not
    yet on the table_0. The task we need to accomplish is to place the glass_0 onto
    the table_0. The robotic arm needs to perform the following steps: First,
    approach and grasp the glass_0 from its current position. Second, lift and move
    the glass_0 toward the table_0. Third, carefully place the glass_0 onto the
    surface of the table_0, ensuring it is stable and properly positioned. No other
    objects need to be moved or manipulated during this task."

```

D.4.3. SUBTASK DECOMPOSITION

A defining characteristic of AGT-World is its structured, graph-based decomposition. By modeling the task space as transitions between simple sub-tasks, we ensure that the decomposition is deterministic across hundreds of demos. Regardless of visual variations in the scene, the logical steps required to satisfy the complex goal remain invariant.

Due to space limitations, this document only shows the names and descriptions of each sub-task within the complex long-horizon tasks. Information such as target objects, support objects, and BDDL names, which are included in the output configuration file, are not presented here. The following are representative outputs for a single demo of each complex long-horizon task:

\mathcal{T}_1 : Transport a glass into a refrigerator.

```

"sub_task_1": {
    "task_activity_name": "open_refrigerator",
    "task_detail_message": "First, the robotic arm needs to approach the handle of
        the refrigerator_0 and rotate to open it.",
    ...
},
"sub_task_2": {
    "task_activity_name": "pick_up_glass",
    "task_detail_message": "Second, pick up the glass_0 from the table_0. The robotic
        arm needs to navigate to the glass_0, approach it, grasp it, and lift it
        from the table_0.",
    ...
},
"sub_task_3": {
    "task_activity_name": "put_glass_into_refrigerator",
    "task_detail_message": "Third, place the glass_0 inside the refrigerator_0. The
        robotic arm needs to navigate to the refrigerator_0, move forward while
        holding the glass_0, and ungrasp to place it inside the refrigerator_0.",
    ...
},
"sub_task_4": {
    "task_activity_name": "close_refrigerator",
    "task_detail_message": "Finally, close the refrigerator_0. The robotic arm needs
        to approach the handle of the refrigerator_0 and rotate to close it.",
    ...
}

```

\mathcal{T}_2 : Place an apple into a refrigerator.

```

"sub_task_1": {
    "task_activity_name": "open_refrigerator",
    "task_detail_message": "First, approach the refrigerator_0 and open its door by
        grasping and rotating the handle."
}

```

```

    ...
},
"sub_task_2": {
    "task_activity_name": "pick_up_apple",
    "task_detail_message": "Second, pick up the apple_0 from the table_0. The robotic arm needs to navigate to the target apple_0, approach it, grasp it, and lift it off the table_0.",
    ...
},
"sub_task_3": {
    "task_activity_name": "put_apple_into_refrigerator",
    "task_detail_message": "Third, carefully place the apple_0 inside the refrigerator_0. The robotic arm needs to navigate to the refrigerator_0, move forward, and release the apple_0 inside the refrigerator_0.",
    ...
},
"sub_task_4": {
    "task_activity_name": "close_refrigerator",
    "task_detail_message": "Finally, close the refrigerator_0 door to complete the task. The robot needs to navigate to the refrigerator_0, get close to the handle, and rotate to close the door.",
    ...
}
}

```

\mathcal{T}_3 : Transfer an apple into a bowl.

```

"sub_task_1": {
    "task_activity_name": "pick_up_apple",
    "task_detail_message": "The robotic arm must first approach and grasp the apple_0 while it is stationary on the countertop of cabinet_0. The target object is apple_0, and the support object is cabinet_0 as the success condition is that the apple_0 is no longer resting on the cabinet_0 surface.",
    ...
},
"sub_task_2": {
    "task_activity_name": "put_apple_into_bowl",
    "task_detail_message": "Then, without releasing the apple_0, the arm must move it over to the bowl_0 on the table_0 and gently release it inside the bowl_0. The target object remains apple_0, but now the support object is bowl_0, as the success condition is that the apple_0 is inside the bowl_0.",
    ...
}

```

\mathcal{T}_4 : Place a cup onto a table.

```

"sub_task_1": {
    "task_activity_name": "pick_up_glass",
    "task_detail_message": "First, the robotic arm must locate and pick up the glass_0 from its current position (near the cabinet or floor level). The robot needs to approach the glass_0, grasp it securely, and lift it off its current surface.",
    ...
},
"sub_task_2": {
    "task_activity_name": "put_glass_on_table",
    "task_detail_message": "Second, the robotic arm must move the glass_0 toward the table_0 and gently place it on the tabletop, ensuring stability. The robot should navigate to the table_0, lower the glass_0 onto its surface, and

```

```

    release it carefully.",
    ...
}
```

D.4.4. OBJECT SIZE ADJUSTMENT

To bridge the gap between reconstructed visual assets and physical robot constraints, we implement a dynamic scaling module. For each subtask, the system identifies the target object and applies a scaling factor calculated from its bounding box extents relative to the robot's parallel gripper width ($\approx 0.06m$).

Detailed Scaling for \mathcal{T}_1 and \mathcal{T}_2 . In complex long-horizon task 1, the target object sequence for each sub-task involves [refrigerator_0: 1.0, glass_0: 0.37, glass_0: 0.37, refrigerator_0: 1.0].

For fixed fixtures like the refrigerator, the scale is set to 1.0 to maintain the room's layout. For the manipulable glass_0 object, a scaling factor of 0.37 was determined in sub-tasks 2 and 3 to ensure the glass diameter was easy to grasp. Finally, we selected the first occurring scaling factors for the refrigerator and the glass, which are 1.0 and 0.37 respectively, and applied these scaling factors.

In complex long-horizon task 2, the target object sequence for each sub-task involves [refrigerator_0: 1.0, apple_0: 0.35, glass_0: 0.4, refrigerator_0: 1.0]. And we select 1.0 and 0.35 for the refrigerator and the apple respectively

Detailed Scaling for \mathcal{T}_3 and \mathcal{T}_4 . In complex long-horizon task 3 and 4, the target object sequence for each sub-task is [apple_0: 0.42, apple_0: 0.42] and [glass_0: 0.4, glass_0: 0.4]. So we use the first occurring scaling factors 0.42 and 0.4 for \mathcal{T}_3 and \mathcal{T}_4 respectively.

D.4.5. BDDL GENERATION (INITIAL STATE AND SUCCESS DETECTION)

The BDDL generation stage defines the logical boundaries of each subtask. The Table 4 shows the representative initial and target (goal) states of the BDDL definitions for these four complex long-horizon tasks, and we also show the representative outputs for a single demo.

Table 4. Initial and goal states for the sub-tasks of our complex long-horizon tasks

Tasks	Subtask Index	Initial State	Target State
\mathcal{T}_1 : Glass→Fridge	1	(not (open refrigerator_0))	(open refrigerator_0)
	2	(ontop glass_0 table_0)	(not (ontop glass_0 table_0))
	3	(inside glass_0 gripper)	(inside glass_0 refrigerator_0)
	4	(open refrigerator_0)	(not (open refrigerator_0))
\mathcal{T}_2 : Apple→Fridge	1	(not (open refrigerator_0))	(open refrigerator_0)
	2	(ontop apple_0 table_0)	(not (ontop apple_0 table_0))
	3	(inside apple_0 gripper)	(inside apple_0 refrigerator_0)
	4	(open refrigerator_0)	(not (open refrigerator_0))
\mathcal{T}_3 : Apple→Bowl	1	(ontop apple_0 cabinet_0)	(not (ontop apple_0 cabinet_0))
	2	(inside apple_0 gripper)	(inside apple_0 bowl_0)
\mathcal{T}_4 : Cup→Table	1	(ontop glass_0 cabinet_0)	(not (ontop glass_0 cabinet_0))
	2	(inside glass_0 gripper)	(ontop glass_0 table_0)

D.4.6. INITIAL ACTION FLOW

The mapping of high-level subtask definitions to executable primitive sequences is a critical step in the AGT-World pipeline. While visual keyframes of these executions are omitted here for brevity, comprehensive video demonstrations of the initial and evolved policies for all tasks are available on our project page (as linked in the Abstract).

Detailed definitions and physical implementations of each atomic primitive (e.g., *APPROACH*, *CONVERGE*, *ARTICULATE*) are provided in Appendix A.2.3. Table 5 summarizes the deterministic initial action sequences generated by our graph-based planner for the four representative complex long-horizon tasks before any self-evolution iterations.

Table 5. Initial action flows for the sub-tasks of our representative complex long-horizon tasks

Tasks	Subtask	Initial Action Flow (Pre-evolution)
T_1	1	APPROACH → CONVERGE → GRASP → ARTICULATE_OPEN → UNGRASP
	2	NAVIGATE_TO_TARGET → APPROACH → CONVERGE → GRASP → LIFT_EEF_UP(0.2)
	3	NAVIGATE_TO_SUPPORT → MOVE_BASE_FORWARD(0.4) → MOVE_EEF_FORWARD(0.1) → UNGRASP
	4	NAVIGATE_TO_TARGET → APPROACH → CONVERGE → GRASP → ARTICULATE_CLOSE(0.0, 0.5) → UNGRASP
T_2	1	APPROACH → CONVERGE → GRASP → ARTICULATE_OPEN(0.0, 0.7) → UNGRASP → RETREAT
	2	NAVIGATE_TO_TARGET → RETREAT → APPROACH → CONVERGE → GRASP → LIFT_EEF_UP(0.2)
	3	NAVIGATE_TO_SUPPORT → MOVE_BASE_FORWARD(0.4) → MOVE_EEF_FORWARD(0.1) → UNGRASP
	4	NAVIGATE_TO_TARGET → APPROACH → CONVERGE → GRASP → ARTICULATE_CLOSE(0.0, 0.7) → UNGRASP
T_3	1	APPROACH → CONVERGE → GRASP → LIFT_EEF_UP(0.2)
	2	NAVIGATE_TO_SUPPORT → MOVE_BASE_FORWARD(0.4) → MOVE_EEF_FORWARD(0.1) → LIFT_EEF_DOWN(0.3) → UNGRASP
T_4	1	APPROACH → CONVERGE → GRASP → LIFT_EEF_UP(0.2)
	2	NAVIGATE_TO_SUPPORT → MOVE_BASE_FORWARD(0.4) → MOVE_EEF_FORWARD(0.1) → LIFT_EEF_DOWN(0.3) → UNGRASP

D.5. Performance of Self-Evolution

In this section, we present the step-by-step evolution trajectory for the four representative complex long-horizon tasks. The Self-Evolution mechanism plays a crucial role in correcting execution failures caused by geometric uncertainties or kinematic constraints that are difficult to resolve with open-loop planning.

We report the evolutionary process for one representative demonstration of each complex long-horizon task. Tables 6, 7, 8, and 9 detail the changes in the action flow across iterations. The ‘‘Iter 0’’ row represents the initial open-loop plan generated by the graph solver. Subsequent iterations show how the VLM refined the sequence by adjusting parameters or inserting new primitives.

Evolution of Task T_1 (Transport Glass into Refrigerator). The evolution process of Task T_1 (placing a glass into the refrigerator) is shown in Table 6. Subtasks 1 and 2 were successfully completed on the first attempt. However, subtask 3 (place the glass) required two iterations of improvement. Initially, the robot collided with the open refrigerator door, causing the door to close and preventing the subsequent tasks from being executed. Therefore, the VLM adjusted the base movement path. After one iteration, the glass was released too high and too far back, so the VLM adjusted the robot arm’s extension range to ensure safe placement in the correct position. Subtask 4 (close the refrigerator) required one iteration of improvement to ensure the refrigerator door was completely closed.

Table 6. Evolutionary Trajectory for Task T_1 : ‘‘Put the cup into the refrigerator’’. Subtasks 1 and 2 succeeded initially. Subtask 3 required 2 iterations to correct placement height and depth. Subtask 4 required 1 iteration to fully close the door.

Subtask	Iter	Action Flow
1	0	APPROACH → CONVERGE → GRASP → ARTICULATE_OPEN → UNGRASP
2	0	NAVIGATE_TO_TARGET → APPROACH → CONVERGE → GRASP → LIFT_EEF_UP(0.2)
3	0	NAVIGATE_TO_SUPPORT → MOVE_BASE_FORWARD(0.4) → MOVE_EEF_FORWARD(0.1) → UNGRASP
	1	NAVIGATE_TO_SUPPORT → MOVE_BASE_FORWARD(0.3) → MOVE_EEF_FORWARD(0.45) → UNGRASP
	2	NAVIGATE_TO_SUPPORT → MOVE_BASE_FORWARD(0.3) → MOVE_EEF_FORWARD(0.45) → MOVE_EEF_FORWARD(0.2) → LIFT_EEF_DOWN(0.3) → UNGRASP
4	0	NAVIGATE_TO_TARGET → APPROACH → CONVERGE → GRASP → ARTICULATE_CLOSE(0.0, 0.5) → UNGRASP
	1	NAVIGATE_TO_TARGET → APPROACH → CONVERGE → GRASP → ARTICULATE_CLOSE(0.0, 0.6) → MOVE_EEF_FORWARD(0.1) → UNGRASP

Evolution of Task T_2 (Place Apple into Refrigerator). Table 7 show the evolution results. Subtask 3 failed initially because the robot could not reach the deep shelf. The evolution process involved significant adjustments to the base position and rotation (TURN_BASE) over 3 iterations to achieve a valid kinematic configuration for placement.

Evolution of Task T_3 (Transfer Apple into Bowl). This evolution details is in Table 8, which required precise positioning to ensure the apple landed *inside* the bowl rather than hitting the rim. Subtask 2 evolved twice: first to adjust the approach angle via TURN_BASE, and second to fine-tune the release height.

Evolution of Task T_4 (Place Cup onto Table) Similar to T_3 , Table 9 shows that placing a cup on a specific spot on the table required adjusting the robot base’s orientation (TURN_BASE) to reach the target zone.

Table 7. Evolutionary Trajectory for Task \mathcal{T}_2 : “Put the apples into the refrigerator”. Subtask 3 underwent 3 iterations, introducing base rotation and finer arm control to navigate the apple onto the fridge shelf.

Subtask	Iter	Action Flow
1	0	APPROACH → CONVERGE → GRASP → ARTICULATE_OPEN(0.0, 0.7) → UNGRASP → RETREAT
2	0	NAVIGATE_TO_TARGET → RETREAT → APPROACH → CONVERGE → GRASP → LIFT_EEF_UP(0.2)
3	0	NAVIGATE_TO_SUPPORT → MOVE_BASE_FORWARD(0.4) → MOVE_EEF_FORWARD(0.1) → UNGRASP
	1	NAVIGATE_TO_SUPPORT → MOVE_BASE_BACKWARD(0.3) → MOVE_EEF_FORWARD(0.4) → MOVE_EEF_FORWARD(0.2) → UNGRASP
	2	NAVIGATE_TO_SUPPORT → MOVE_BASE_BACKWARD(0.3) → MOVE_EEF_FORWARD(0.4) → TURN_BASE_LEFT(45) → MOVE_EEF_FORWARD(0.2) → UNGRASP
	3	NAVIGATE_TO_SUPPORT → MOVE_BASE_BACKWARD(0.3) → MOVE_EEF_FORWARD(0.4) → TURN_BASE_LEFT(45) → MOVE_EEF_FORWARD(0.3) → LIFT_EEF_DOWN(0.2) → UNGRASP
4	0	NAVIGATE_TO_TARGET → APPROACH → CONVERGE → GRASP → ARTICULATE_CLOSE(0.0, 0.7) → UNGRASP

Table 8. Evolutionary Trajectory for Task \mathcal{T}_3 : “Pick the apple into the bowl”. The placement subtask (Subtask 2) required 2 iterations to prevent collision with the bowl’s rim.

Subtask	Iter	Action Flow
1	0	APPROACH → CONVERGE → GRASP → LIFT_EEF_UP(0.2)
2	0	NAVIGATE_TO_SUPPORT → MOVE_BASE_FORWARD(0.4) → MOVE_EEF_FORWARD(0.1) → LIFT_EEF_DOWN(0.3) → UNGRASP
	1	NAVIGATE_TO_SUPPORT → MOVE_BASE_BACKWARD(0.15) → MOVE_EEF_FORWARD(0.4) → TURN_BASE_LEFT(15) → MOVE_EEF_FORWARD(0.1) → LIFT_EEF_DOWN(0.4) → UNGRASP
	2	NAVIGATE_TO_SUPPORT → MOVE_BASE_BACKWARD(0.3) → MOVE_EEF_FORWARD(0.2) → TURN_BASE_RIGHT(20) → MOVE_EEF_FORWARD(0.25) → LIFT_EEF_DOWN(0.4) → UNGRASP

Table 9. Evolutionary Trajectory for Task \mathcal{T}_4 : “Put the cup on the table”. Subtask 2 required 2 iterations, heavily relying on base rotation to align with the table surface.

Subtask	Iter	Action Flow
1	0	APPROACH → CONVERGE → GRASP → LIFT_EEF_UP(0.2)
2	0	NAVIGATE_TO_SUPPORT → MOVE_BASE_FORWARD(0.4) → MOVE_EEF_FORWARD(0.1) → LIFT_EEF_DOWN(0.3) → UNGRASP
	1	NAVIGATE_TO_SUPPORT → TURN_BASE_RIGHT(60) → MOVE_EEF_FORWARD(0.4) → MOVE_EEF_FORWARD(0.1) → LIFT_EEF_DOWN(0.3) → UNGRASP
	2	NAVIGATE_TO_SUPPORT → TURN_BASE_RIGHT(60) → MOVE_EEF_FORWARD(0.4) → MOVE_EEF_FORWARD(0.2) → LIFT_EEF_DOWN(0.3) → UNGRASP

VLM Reasoning Process. To illustrate the decision-making capability of the Self-Evolution mechanism, we provide the raw reasoning outputs for Task \mathcal{T}_1 in the box below. This includes the step-wise critiques \mathbf{m} and the final Global Supervisor reasoning.

First, subtask 3 underwent two iterations, and the output of all iterations are:

```

"iter_1": {
    "VLM-Observation": {
        "Step 0 observation (4 frames)": "The robot base navigates to the support (refrigerator), positioning itself near the open refrigerator door. The refrigerator door remains open throughout, and no collision or environmental change is observed during this step.",
        "Step 1 observation (4 frames)": "The robot base moves forward 0.45 meters toward the refrigerator. During this motion, the robotic arm collides with the open refrigerator door, causing it to swing shut partially, which alters the environment and obstructs access to the refrigerator compartment.",
        "Step 2 observation (2 frames)": "The robot performs the UNGRASP action while its arm is positioned near the now partially closed refrigerator door. No further collision occurs, but the glass is not placed inside the refrigerator due to the obstructed access caused by the door's position."
    }
}

```

```

        The environment remains unchanged during this step."
    },
    "reason": "During the execution of 'put_glass_into_refrigerator', the robotic arm
    collided with the open refrigerator door while performing 'MOVE_BASE_FORWARD'
    ', causing the door to close partially and blocking access to the compartment.
    Therefore, before 'MOVE_BASE_FORWARD', the following step should be added: '
    MOVE_BASE_LEFT 0.3m' to clear the door swing path.",
    "new_sequence": [18, {"15": 0.3}, {"13": 0.45}, 5]
},
"iter_2": {
    "VLM-Observation": {
        "Step 0 observation (4 frames)": "The robot base navigates toward the
        refrigerator, positioning itself so the arm can reach the open door. No
        collision occurs, and the refrigerator door remains open; the environment
        status is unchanged.",
        "Step 1 observation (3 frames)": "The robot base moves left by 0.3 meters,
        repositioning the arm slightly away from the refrigerator door. No
        collision occurs, and the refrigerator door remains open; no environmental
        changes are observed.",
        "Step 2 observation (4 frames)": "The robot base moves forward by 0.45 meters,
        bringing the arm closer to the refrigerator. No collision occurs, and the
        refrigerator door remains open; no environmental changes are observed.",
        "Step 3 observation (2 frames)": "The robot opens its gripper to release the
        glass, but the glass is not visible inside the refrigerator, indicating it
        was not placed successfully. No collision occurs, and the refrigerator
        door remains open; no environmental changes are observed."
    },
    "reason": "The task failed because after moving the base forward, the robotic arm
    did not extend far enough into the refrigerator to place the glass inside
    before releasing it. The UNGRASP action occurred while the gripper was still
    outside the refrigerator compartment. Therefore, after 'MOVE_BASE_FORWARD',
    the following steps should be added: 1. 'MOVE_EEF_FORWARD 0.2m' to extend the
    arm into the refrigerator, and 2. 'LIFT_EEF_DOWN 0.3m' to lower the glass to
    a safe placement height inside the refrigerator.",
    "new_sequence": [18, {"15": 0.3}, {"13": 0.45}, {"9": 0.2}, {"8": 0.3}, 5]
}
    
```

Next, here are the output results for subtask 4:

```

"iter_1": {
    "VLM-Observation": {
        "Step 0 observation (5 frames)": "The robot successfully navigates to the
        refrigerator, positioning itself beside the open door without hitting any
        obstacles. The environment remains unchanged during this step; the
        refrigerator door stays open, and no unintended movements or collisions
        occur.",
        "Step 1 observation (1 frames)": "The robot arm extends toward the
        refrigerator handle in a controlled manner, maintaining clearance from
        surrounding objects. No collision occurs, and the refrigerator door
        remains open without any unintended movement or environmental change.",
        "Step 2 observation (1 frames)": "The robot arm finely adjusts its position to
        align precisely with the refrigerator handle, showing no contact with
        surrounding objects. The refrigerator door remains open and stationary,
        with no environmental changes or collisions observed.",
        "Step 3 observation (1 frames)": "The robot gripper successfully closes around
        the refrigerator handle without colliding with any surrounding objects.
        The refrigerator door remains open and stationary, with no unintended
        environmental changes observed during the grasp.",
        "Step 4 observation (6 frames)": "The robot arm attempts to close the
        refrigerator door by pulling the handle, but the door does not fully shut
    }
}
    
```

```

        and appears to be obstructed or misaligned. No collision with surrounding
        objects is observed, but the environment status changes partially - the
        door moves slightly but fails to reach a fully closed position, indicating
        an incomplete articulation.",
        "Step 5 observation (2 frames)": "The robot opens its gripper to release the
        refrigerator handle, with no contact or collision observed. The
        refrigerator door remains partially open and does not move further during
        ungrasping, indicating that the failure to fully close occurred prior to
        this step."
    },
    "reason": "The failure occurred during the 'ARTICULATE_CLOSE' step. Although the
        robot successfully grasped the handle and attempted to close the door, the
        door did not fully shut, likely due to insufficient pulling force or
        misalignment in the articulation range. To correct this, we should extend the
        articulation range slightly beyond 0.5 and add a small forward motion of the
        EEF before ungrasping to ensure full closure.",
    "new_sequence": [17, 1, 2, 3, {"19": [0.0, 0.6]}, {"9": 0.1}, 5]
}
    
```

D.6. Failure Details and Analysis

D.6.1. PERFORMANCE VARIANCE ACROSS VLM ARCHITECTURES

We conducted a comparative study on the self-evolution performance of three VLMs: **Gemini-3-Flash**, **GPT-5.2**, and **Qwen3-VL** (specifically, the open-source model *qwen3-vl-235b-22a-thinking*). While all models demonstrated reasoning capabilities, their evolution strategies exhibited distinct characteristics:

- **Qwen3-VL (Conservative Strategy):** This model tends to be conservative in its modifications. Its proposed changes often involve minimal adjustments, such as tweaking a single parameter or adding just one or two atomic actions. While this ensures stability, Qwen3-VL frequently fails to identify “stuck” situations, where the robot is physically blocked but not in collision, resulting in minor updates that do not resolve the root cause.
- **Gemini-3-Flash (Aggressive Strategy):** Gemini-3-Flash exhibits a more aggressive and perceptive reasoning style. It is often capable of identifying subtle geometric constraints, such as the robot arm grazing the edge of a fridge door. Consequently, it proposes significant modifications, such as changing a movement parameter from around 0.3m to around 0.8m. However, given the offline nature of our evolution mechanism (where the VLM cannot interactively query state during reasoning), these large-scale parameter jumps sometimes degrade accuracy, causing the robot to deviate from the correct target position.
- **GPT-5.2 (Redundant Strategy):** GPT-5.2 shows a tendency to over-complicate solutions. It frequently stacks new actions onto the existing sequence rather than refining the current ones. This often leads to a “death spiral” where the action sequence grows to over 10 steps. As the sequence length increases, the probability of cumulative execution error rises, making success increasingly difficult despite valid high-level logic.

D.6.2. CASE STUDIES ON PERSISTENT FAILURES

Qualitative inspection of failure cases reveals that errors are rarely due to high-level logic. Instead, they stem from low-level kinematic constraints, such as the robotic arm reaching a singularity when confined against the fridge side, or the hard-coded action primitives lacking the reflexivity to compensate for minor grasping errors.

Case 1: Kinematic Obstruction in Task T_1 (Glass \rightarrow Fridge). Figure 9 shows the first 4 iterations of subtask 3 (placing the glass into the refrigerator), which ultimately failed after 5 iterations. The visual record shows the robot attempting to extend its arm deep into the refrigerator.

As observed in the figures, the root cause is not the arm extension parameter, but the base positioning. The robotic arm link is physically blocked by the left side of the refrigerator frame, preventing the arm from extending fully. This type of collision is subtle and difficult for the VLM to perceive from the standard camera views.

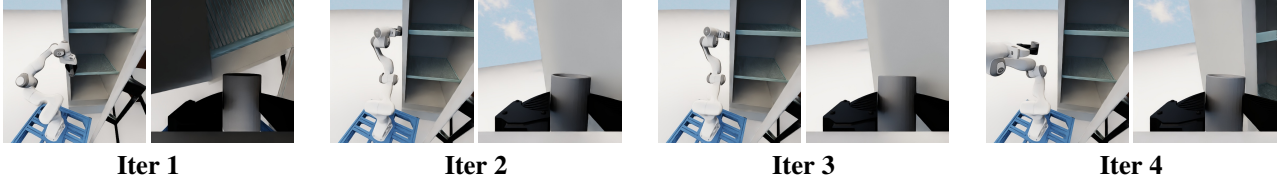


Figure 9. Failure Analysis for \mathcal{T}_1 Subtask 3. Despite 4 rounds of evolution (Iter 5 also failed), the robot consistently fails to insert the glass. The root cause, visible in the Overhead View, is that the lower link of the robotic arm collides with the left wall of the refrigerator, preventing the end-effector from advancing. This kinematic constraint is difficult for the VLM to diagnose from 2D images, as it requires a subtle backward adjustment of the mobile base to clear the singularity, which is a correction that iterative parameter tuning failed to find.

Case 2: Precision Placing in Task \mathcal{T}_3 (Apple → Bowl). Figure 10 depicts a failure in Subtask 2 (Place apple into bowl). The challenge here is fine-grained spatial alignment.



Figure 10. Failure Analysis for \mathcal{T}_3 Subtask 2. The robot struggles to align the apple directly above the bowl. Over 4 iterations, the VLM attempts to correct the drift, but lacks the precision to calculate the exact offset. The open-loop nature means the VLM oscillates between over-correcting (moving too far left) and under-correcting, failing to find the "sweet spot" within the limited iteration budget.

As shown in the iteration history, the VLM struggles to calculate the exact spatial offset required to center the gripper over the bowl. Since our method generates the next plan offline based on static visual feedback, the VLM cannot rely on real-time continuous servoing. This results in an oscillation where the robot either adjusts too little (incremental trial-and-error) or modifies parameters too aggressively, missing the target window.